

---

# Light Unbalanced Optimal Transport

---

**Milena Gazdieva**

Skolkovo Institute of Science and Technology  
Moscow, Russia  
milena.gazdieva@skoltech.ru

**Arip Asadulaev**

ITMO University  
Artificial Intelligence Research Institute  
Moscow, Russia  
asadulaev@airi.net

**Evgeny Burnaev**

Skolkovo Institute of Science and Technology  
Artificial Intelligence Research Institute  
Moscow, Russia  
e.burnaev@skoltech.ru

**Alexander Korotin**

Skolkovo Institute of Science and Technology  
Artificial Intelligence Research Institute  
Moscow, Russia  
a.korotin@skoltech.ru

## Abstract

While the continuous Entropic Optimal Transport (EOT) field has been actively developing in recent years, it became evident that the classic EOT problem is prone to different issues like the sensitivity to outliers and imbalance of classes in the source and target measures. This fact inspired the development of solvers that deal with the *unbalanced* EOT (UEOT) problem – the generalization of EOT allowing for mitigating the mentioned issues by relaxing the marginal constraints. Surprisingly, it turns out that the existing solvers are either based on heuristic principles or heavy-weighted with complex optimization objectives involving several neural networks. We address this challenge and propose a novel theoretically-justified, lightweight, unbalanced EOT solver. Our advancement consists of developing a novel view on the optimization of the UEOT problem yielding tractable and a non-minimax optimization objective. We show that combined with a light parametrization recently proposed in the field our objective leads to a fast, simple, and effective solver which allows solving the continuous UEOT problem in minutes on CPU. We prove that our solver provides a universal approximation of UEOT solutions and obtain its generalization bounds. We give illustrative examples of the solver’s performance.

## 1 Introduction

The computational *optimal transport* (OT) has proven to be a powerful tool for solving various popular tasks, e.g., image-to-image translation [66, 17, 48, 28], image generation [65, 13, 7] and biological data transfer [5, 40, 64]. Historically, the majority of early works in the field were built upon solving the OT problem between discrete probability measures [10, 51]. Only recently the advances in the field of generative models have led to explosive interest from the ML community in developing the **continuous** OT solvers, see [36] for a survey. The setup of this problem assumes that the learner needs to estimate the OT plan between continuous measures given only empirical samples of data from them. Due to convexity-related issues of OT problem [38], many works consider the EOT problem, i.e., use *entropy* regularizers which guarantee, e.g., the uniqueness of learned plans.

Meanwhile, researches attract attention to other shortcomings of the classic OT problem. It enforces hard constraints on the marginal measures and, thus, does not allow for mass variations. As a result, OT shows high sensitivity to an imbalance of classes and outliers in the source and target measures [4] which are almost inevitable for large-scale datasets. To overcome these issues, it is common to consider extensions of the OT problem, e.g., unbalanced OT/EOT (UOT/UEOT) [8, 41]. The unbalanced OT/EOT formulations allow for variation of total mass by relaxing the marginal constraints through the use of divergences.

The scope of our paper is the continuous UEOT problem. It seems that in this field, a solver that is fast, light, and theoretically justified has not yet been developed. Indeed, many of the existing solvers follow a kind of heuristical principles and are based on the solutions of discrete OT. For example, [43] uses a regression to interpolate the discrete solutions, and [16, 34] build a flow matching upon them. Almost all of the other solvers [9, 68] employ several neural networks with many hyper-parameters and require time-consuming optimization procedures. We solve the aforementioned shortcomings by introducing a novel lightweight solver that can play the role of a simple baseline for unbalanced EOT.

**Contributions.** We develop a novel *lightweight* solver to estimate continuous **unbalanced** EOT couplings between probability measures (§4). Our solver has a non-minimax optimization objective and employs the Gaussian mixture parametrization for the UEOT plans. We provide the generalization bounds for our solver (§4.4) and experimentally test it on several tasks (§5.1, §5.2).

**Notations.** We work in the Euclidian space  $(\mathbb{R}^d, \|\cdot\|)$ . We use  $\mathcal{P}_{2,ac}(\mathbb{R}^d)$  (or  $\mathcal{M}_{2,+}(\mathbb{R}^d)$ ) to denote the set of absolutely continuous Borel probability (or non-negative) measures on  $\mathbb{R}^d$  with finite second moment and differential entropy. We use  $\mathcal{C}_2(\mathbb{R}^d)$  to denote the space of all *continuous* functions  $\zeta : \mathbb{R}^d \rightarrow \mathbb{R}$  for which  $\exists a = a(\xi), b = b(\xi)$  such that  $\forall x \in \mathbb{R}^d : |\zeta(x)| \leq a + b\|x\|^2$ . Its subspace of functions which are additionally *bounded from above* is denoted as  $\mathcal{C}_{2,b}(\mathbb{R}^d)$ . For any  $p \in \mathcal{P}_{2,ac}(\mathbb{R}^d)$  (or  $\mathcal{M}_{2,+}(\mathbb{R}^d)$ ), we use  $p(x)$  to denote its density at a point  $x \in \mathbb{R}^d$ . For a given measure  $\gamma \in \mathcal{M}_{2,+}(\mathbb{R}^d \times \mathbb{R}^d)$ , we denote its total mass by  $\|\gamma\|_1 \stackrel{\text{def}}{=} \int_{\mathbb{R}^d \times \mathbb{R}^d} \gamma(x, y) dx dy$ . We use  $\gamma_x(x), \gamma_y(y)$  to denote the marginals of  $\gamma(x, y)$ . They satisfy the equality  $\|\gamma_x\|_1 = \|\gamma_y\|_1 = \|\gamma\|_1$ . We write  $\gamma(y|x)$  to denote the conditional *probability* measure. Each such measure has a unit total mass. We use  $\bar{f}$  to denote the Fenchel conjugate of a function  $f$ :  $\bar{f}(t) = \sup_{u \in \mathbb{R}^d} \{ut - f(u)\}$ . We use  $\mathbb{I}_A$  to denote the convex indicator of a set  $A$ , i.e.,  $\mathbb{I}_A(x) = 0$  if  $x \in A$ ;  $\mathbb{I}_A(x) = +\infty$  if  $x \notin A$ .

## 2 Background

Here we give an overview of the relevant entropic optimal transport (EOT) concepts. For additional details on balanced EOT, we refer to [10, 24, 51], unbalanced EOT - to [8, 41].

**$f$ -divergences for positive measures.** For *positive* measures  $\mu_1, \mu_2 \in \mathcal{M}_{2,+}(\mathbb{R}^d)$  and a lower semi-continuous function  $f : \mathbb{R} \rightarrow \mathbb{R} \cup \{\infty\}$ ,  $f$ -divergence between  $\mu_1, \mu_2$  is defined by:

$$\mathcal{D}_f(\mu_1 \|\mu_2) \stackrel{\text{def}}{=} \int_{\mathbb{R}^d} f\left(\frac{\mu_1(x)}{\mu_2(x)}\right) \mu_2(x) dx.$$

We consider  $f(t)$  which are convex, non-negative and attain zero uniquely when  $t = 1$ . In this case,  $\mathcal{D}_f$  is a valid measure of dissimilarity between two positive measures (see Appendix C for details). This means that  $\mathcal{D}_f(\mu_1 \|\mu_2) \geq 0$  and  $\mathcal{D}_f(\mu_1 \|\mu_2) = 0$  if and only if  $\mu_1 = \mu_2$ .

Kullback-Leibler divergence  $\mathcal{D}_{\text{KL}}$  [8, 60], is a particular case of such  $f$ -divergence for positive measures. It has a generator function  $f_{\text{KL}}(t) \stackrel{\text{def}}{=} t \log t - t + 1$ . Its convex conjugate  $\bar{f}_{\text{KL}}(t) = \exp(t) - 1$ . Another example is the  $\chi^2$ -divergence  $\mathcal{D}_{\chi^2}$  which is generated by the  $f_{\chi^2}(t) = \mathbb{I}_{t < 0} \cdot \infty + \mathbb{I}_{t \geq 0} \cdot (t-1)^2$ . The convex conjugate of this function is  $\bar{f}_{\chi^2}(t) = \mathbb{I}_{t < -2} \cdot (-1) + \mathbb{I}_{t \geq -2} \cdot (\frac{1}{4}t^2 + t)$ .

**Entropy for positive measures.** For  $\mu \in \mathcal{M}_{2,+}(\mathbb{R}^d)$ , its entropy [8] is given by

$$H(\mu) \stackrel{\text{def}}{=} - \int_{\mathbb{R}^d} \mu(x) \log \mu(x) dx + \int_{\mathbb{R}^d} \mu(x) dx. \quad (1)$$

When  $\mu \in \mathcal{P}_{2,ac}(\mathbb{R}^d)$ , i.e.,  $\int_{\mathbb{R}^d} \mu(x) dx = 1$ , equation (1) is the usual differential entropy minus 1.

**Classic EOT formulation (with the quadratic cost).** Consider two probability measures  $p \in \mathcal{P}_{2,ac}(\mathbb{R}^d), q \in \mathcal{P}_{2,ac}(\mathbb{R}^d)$ . For  $\varepsilon > 0$ , the EOT problem between  $p$  and  $q$  is

$$\min_{\pi \in \Pi(p,q)} \int_{\mathbb{R}^d} \int_{\mathbb{R}^d} \frac{\|x-y\|^2}{2} \pi(x,y) dx dy - \varepsilon H(\pi), \quad (2)$$

where  $\Pi(p, q)$  is the set of probability measures  $\pi \in \mathcal{P}_{2,ac}(\mathbb{R}^d \times \mathbb{R}^d)$  with marginals  $p, q$  (transport plans). Plan  $\pi^*$  attaining the minimum exists, it is unique and called the *EOT plan*.

Classic EOT imposes hard constraints on the marginals which leads to several issues, e.g., sensitivity to outliers [4], inability to handle potential measure shifts such as class imbalances in the measures  $p, q$ . The UEOT problem [68, 9] overcomes these issues by relaxing the marginal constraints [60].

Solver	Problem	Principles	What recovers?	Limitations
[68]	UOT	Solves $c$ -transform based semi-dual max-min reformulation of UOT using neural nets	Scaling factor $\gamma^*(x)/p(x)$ and stochastic OT map $T^*(x, z)$	Complex max-min objective; 3 neural networks
[43]	Custom UOT	Regression on top of discrete EOT between re-balanced measures combined with ICNN-based solver [45]	Scaling factors and OT maps between re-scaled measures	Heuristically uses minibatch OT approximations
[9]	UOT	Solves semi-dual max-min reformulation of UOT using neural nets	Stochastic UOT map $T^*(x, z)$	Complex max-min objective; 2 neural networks
[16]	UEOT	Flow Matching on top of discrete UEOT using neural nets	Parametrized vector field $(v_t, \theta)_{t \in [0, 1]}$ to transport the mass	Heuristically uses minibatch OT approximations
[34]	UEOT	Conditional Flow Matching on top of discrete EOT between re-balanced measures using neural nets	Scaling factors and parametrized conditional vector field $(v_t, \theta)_{t \in [0, 1]}$ to transport the mass between re-scaled measures	Heuristically uses minibatch OT approximations
U-LightOT (ours)	UEOT	Solves non-minimax reformulation of dual UEOT using Gaussian Mixtures	Density of UEOT plan $\gamma^*$ together with light procedure to sample $x \sim \gamma_x^*(\cdot)$ and $y \sim \gamma_y^*(\cdot x)$	Restricted to Gaussian Mixture parametrization

Table 1: Comparison of the principles of existing UOT/UEOT solvers and **our** proposed light solver.

**Unbalanced EOT formulation (with the quadratic cost).** Let  $D_{f_1}$  and  $D_{f_2}$  be two  $f$ -divergences over  $\mathbb{R}^d$ . For two probability measures  $p \in \mathcal{P}_{2,ac}(\mathbb{R}^d)$ ,  $q \in \mathcal{P}_{2,ac}(\mathbb{R}^d)$  and  $\varepsilon > 0$ , the unbalanced EOT problem between  $p$  and  $q$  consists of finding a minimizer of

$$\inf_{\gamma \in \mathcal{M}_{2,+}(\mathbb{R}^d \times \mathbb{R}^d)} \int_{\mathbb{R}^d} \int_{\mathbb{R}^d} \frac{\|x - y\|^2}{2} \gamma(x, y) dx dy - \varepsilon H(\gamma) + D_{f_1}(\gamma_x \| p) + D_{f_2}(\gamma_y \| q). \quad (3)$$

Here the minimum is attained for a unique  $\gamma^*$  which is called the *unbalanced optimal entropic* (UEOT) plan. Typical choices of  $f_i$  ( $i \in [1, 2]$ ) are  $f_i(a) = \tau_i f_{\text{KL}}(a)$  or  $f_i(x) = \tau_i f_{\chi^2}(a)$  ( $\tau_i > 0$ ) yielding the scaled  $D_{\text{KL}}$  and  $D_{\chi^2}$ , respectively. In this case, the bigger  $\tau_1$  ( $\tau_2$ ) is, the more  $\gamma_x$  ( $\gamma_y$ ) is penalized for not matching the corresponding marginal distribution  $p$  ( $q$ ).

*Remark.* The balanced EOT problem (2) is a special case of (3). Indeed, let  $f_1$  and  $f_2$  be the convex indicators of  $\{1\}$ , i.e.,  $f_1(x) = f_2(x) = \mathbb{I}_{x=1} \cdot 0 + \mathbb{I}_{x \neq 1} \cdot \infty$ . Then the  $f$ -divergences  $D_{f_1}(\gamma_x \| p)$  and  $D_{f_2}(\gamma_y \| q)$  become infinity if  $p \neq \gamma_x$  or  $q \neq \gamma_y$ , and become zeros otherwise.

**Dual form of unbalanced EOT problem** (3) is formulated as follows

$$\sup_{(\phi, \psi)} \left\{ -\varepsilon \int_{\mathbb{R}^d} \int_{\mathbb{R}^d} \exp\left\{ \frac{1}{\varepsilon} (\phi(x) + \psi(y) - \frac{\|x - y\|^2}{2}) \right\} dx dy - \int_{\mathbb{R}^d} \bar{f}_1(-\phi(x)) p(x) dx - \int_{\mathbb{R}^d} \bar{f}_2(-\psi(y)) q(y) dy \right\}. \quad (4)$$

Potentials  $\phi^*$ ,  $\psi^*$  delivering maximum to (4) have the following connection with the solution of the primal unbalanced problem (3):

$$\gamma^*(x, y) = \exp\left\{ \frac{\phi^*(x)}{\varepsilon} \right\} \exp\left\{ -\frac{\|x - y\|^2}{2\varepsilon} \right\} \exp\left\{ \frac{\psi^*(y)}{\varepsilon} \right\}. \quad (5)$$

For our further purposes, we need to consider potentials  $(\phi, \psi)$  in problem (4) which belong to the space  $C_{2,b}(\mathbb{R}^d) \times C_{2,b}(\mathbb{R}^d)$ . Since established variants of dual forms [8] typically correspond to other functional spaces, we derive and theoretically justify the *dual problem* (4) in Appendix A.3.

**Computational UEOT setup.** Analytical solution for the *unbalanced* EOT problem is, in general, not known.<sup>1</sup> Moreover, in real-world setups where unbalanced EOT is applicable, the measures  $p, q$  are typically not available explicitly but only through their empirical samples (datasets).

We assume that data measures  $p, q \in \mathcal{P}_{2,ac}(\mathbb{R}^d)$  are unknown and accessible only by a limited number of i.i.d. empirical samples  $\{x_0, \dots, x_N\} \sim p$ ,  $\{y_0, \dots, y_M\} \sim q$ . We aim to approximate the optimal UEOT plans solving (3) between the entire measures  $p, q$ . The recovered plans should allow the out-of-sample estimation, i.e., generation of samples from  $\gamma^*(\cdot|x^{\text{new}})$  where  $x^{\text{new}}$  is a new test point (not necessarily present in the train data). Optionally, one may require the ability to sample from  $\gamma_x^*$ .

The described setup is typically called the *continuous EOT* and should not be twisted up with the *discrete EOT* [51, 10]. There the aim is to recover the (unbalanced) EOT plan between the empirical measures  $\hat{p} = \frac{1}{N} \sum_{i=1}^N \delta_{x_i}$ ,  $\hat{q} = \frac{1}{M} \sum_{j=1}^M \delta_{y_j}$  and the out-of-sample estimations are typically not needed.

### 3 Related Work

Nowadays, the sphere of continuous OT/EOT solvers is actively developing. Some of the early works related to this topic utilize OT cost as the loss function [27, 25, 2]. These approaches are not relevant to us as they do not learn OT/EOT maps (or plans). We refer to [37] for a detailed review.

<sup>1</sup>Analytical solutions are known only for some specific cases. For example, [32] consider the case of Gaussian measures and UEOT problem with  $D_{\text{KL}}$  divergence instead of differential entropy. This setup differs from ours.

At the same time, there exist a large amount of works within the discrete OT/EOT setup [10, 15, 67, 49], see [51] for a survey. We again emphasize that solvers of this type are not relevant to us as they construct discrete matching between the given (train) samples and typically do not provide a generalization to the new unseen (test) data. Only recently ML community started developing out-of-sample estimation procedures based on discrete/batched OT. For example, [19, 54, 31, 14, 46, 55] mostly develop such estimators using the barycentric projections of the discrete EOT plans. Though these procedures have nice theoretical properties, their scalability remains unclear.

**Balanced OT/EOT solvers.** There exists a vast amount of neural solvers for continuous OT problem. Most of them learn the OT maps (or plans) via solving saddle point optimization problems [3, 18, 35, 22, 58, 48]. Though the recent works [28, 59, 11, 39, 30] tackle the EOT problem (2), they consider its balanced version. Hence they are not relevant to us. Among these works, only [39, 30] evade non-trivial training/inference procedures and are ideologically the closest to ours. The difference between them consists of the particular loss function used. In fact, **our paper** proposes the solver which subsumes these solvers and generalizes them for the unbalanced case. The derivation of our solver is non-trivial and requires solid mathematical apparatus, see §4.

**Unbalanced OT/EOT solvers.** A vast majority of early works in this field tackle the discrete UOT/UEOT setup [6, 20, 52] but the principles under their construction are not easy to generalize to the continuous setting. Thus, many of the recent papers that tackle the continuous unbalanced OT/EOT setup employ discrete solutions in the construction of their solvers. For example, [43] regress neural network on top of scaling factors obtained using the discrete UEOT while simultaneously learning the continuous OT maps using an ICNN method [45]. In [16] and [34], the authors implement Flow Matching [42, FM] and conditional FM on top of the discrete UEOT plans, respectively. The algorithm of the latter consists of regressing neural networks on top of scaling factors and simultaneously learning a conditional vector field to transport the mass between re-balanced measures. Despite the promising practical performance of these solvers, it is still unclear to what extent such approximations of UEOT plans are theoretically justified.

The recent papers [68, 9] are more related to our study as they do not rely on discrete OT approximations of the transport plan. However, they have non-trivial minimax optimization objectives solved using *complex* GAN-style procedures. Thus, these GANs often lean on heavy neural parametrization, may incur instabilities during training, and require careful hyperparameter selection [44].

For completeness, we also mention other papers which are only slightly relevant to us. For example, [23] considers incomplete OT which relaxes only one of the OT marginal constraints and is less general than the unbalanced OT. Other works [12, 4] incorporate unbalanced OT into the training objective of GANs aimed at generating samples from noise.

In contrast to the listed works, our paper proposes a *theoretically justified and lightweight* solver to the UEOT problem, see Table 1 for the detailed comparison of solvers.

## 4 Light Unbalanced OT Solver

In this section, we derive the optimization objective (§4.1) of our U-LightOT solver, present practical aspects of training and inference procedures (§4.2) and derive the generalization bounds for our solver (§4.4). We provide the *proofs of all theoretical results* in Appendix A.

### 4.1 Derivation of the Optimization Objective

Following the learning setup described above, we aim to get a parametric approximation  $\gamma_{\theta, \omega}$  of the UEOT plan  $\gamma^*$ . Here  $\theta, \omega$  are the model parameters to learn and it will be clear later why we split them into two groups. To recover  $\gamma_{\theta, \omega} \approx \gamma^*$ , our aim is to learn  $\theta, \omega$  by directly minimizing the  $D_{\text{KL}}$  divergence between  $\gamma_{\theta, \omega}$  and  $\gamma^*$ :

$$D_{\text{KL}}(\gamma^* \parallel \gamma_{\theta, \omega}) \rightarrow \min_{(\theta, \omega)}. \quad (6)$$

The main difficulty of this optimizing objective (6) is obvious: the UEOT plan  $\gamma^*$  is *unknown*. Fortunately, below we show that one still can optimize (6) without knowing  $\gamma^*$ .

Recall that the optimal UEOT plan  $\gamma^*$  has the form (5). We first make some changes of the variables. Specifically, we define  $v^*(y) \stackrel{\text{def}}{=} \exp\{\frac{2\psi^*(y) - \|y\|^2}{2\varepsilon}\}$ . Formula (5) now reads as

$$\gamma^*(x, y) = \exp\{\frac{2\phi^*(x) - \|x\|^2}{2\varepsilon}\} \exp\{\frac{\langle x, y \rangle}{\varepsilon}\} v^*(y) \implies \gamma^*(y|x) \propto \exp\{\frac{\langle x, y \rangle}{\varepsilon}\} v^*(y). \quad (7)$$

Since the conditional plan has the unit mass, we may write

$$\gamma^*(y|x) = \exp\left\{\frac{\langle x, y \rangle}{\varepsilon}\right\} \frac{v^*(y)}{c_{v^*}(x)} \quad (8)$$

where  $c_{v^*}(x) \stackrel{\text{def}}{=} \int_{\mathbb{R}^d} \exp\left\{\frac{\langle x, y \rangle}{\varepsilon}\right\} v^*(y) dy$  is the normalization constant ensuring that  $\int_{\mathbb{R}^d} \gamma^*(y|x) dy = 1$ .

Consider the decomposition  $\gamma^*(x, y) = \gamma_x^*(x) \gamma^*(y|x)$ . It shows that to obtain parametrization for the entire plan  $\gamma^*(x, y)$ , it is sufficient to consider parametrizations for its left marginal  $\gamma_x^*$  and the conditional measure  $\gamma^*(y|x)$ . Meanwhile, equation (8) shows that *conditional measures  $\gamma^*(\cdot|x)$  are entirely described by the variable  $v^*$* . We use these observations to parametrize  $\gamma_{\theta, w}$ . We set

$$\gamma_{\theta, w}(x, y) \stackrel{\text{def}}{=} u_w(x) \gamma_{\theta}(y|x) = u_w(x) \frac{\exp\{\langle x, y \rangle / \varepsilon\} v_{\theta}(y)}{c_{\theta}(x)}, \quad (9)$$

where  $u_w$  and  $v_{\theta}$  parametrize marginal measure  $\gamma_x^*$  and the variable  $v^*$ , respectively. In turn, the constant  $c_{\theta}(x) \stackrel{\text{def}}{=} \int_{\mathbb{R}^d} \exp\left\{\frac{\langle x, y \rangle}{\varepsilon}\right\} v_{\theta}(y) dy$  is the parametrization of  $c_{v^*}(x)$ . Next, we demonstrate our **main result** which shows that the optimization of (6) can be done *without* the access to  $\gamma^*$ .

**Theorem 4.1** (Tractable form of  $D_{\text{KL}}$  minimization). *Assume that  $\gamma^*$  is parametrized using (9). Then the following bound holds:  $\varepsilon D_{\text{KL}}(\gamma^* \|\gamma_{\theta, w}) \leq \mathcal{L}(\theta, w) - \mathcal{L}^*$ , where*

$$\mathcal{L}(\theta, w) \stackrel{\text{def}}{=} \int_{\mathbb{R}^d} \bar{f}_1(-\varepsilon \log \frac{u_w(x)}{c_{\theta}(x)} - \frac{\|x\|^2}{2}) p(x) dx + \int_{\mathbb{R}^d} \bar{f}_2(-\varepsilon \log v_{\theta}(y) - \frac{\|y\|^2}{2}) q(y) dy + \varepsilon \|u_w\|_1, \quad (10)$$

and constant  $(-\mathcal{L}^*)$  is the optimal value of the dual form (4). The bound is **tight** in the sense that it turns to 0 = 0 when  $v_{\theta}(y) = \exp\{2\psi^*(y) - \|y\|^2/2\varepsilon\}$  and  $u_w(x) = \exp\{2\phi^*(x) - \|x\|^2/2\varepsilon\}$ .

In fact, (10) is the dual form (4) but with potentials  $(\phi, \psi)$  expressed through  $u_w, v_{\theta}$  (and  $c_{\theta}$ ):

$$\phi(x) \leftarrow \phi_{\theta, w}(x) = \varepsilon \log \frac{u_w(x)}{c_{\theta}(x)} + \frac{\|x\|^2}{2}, \quad \psi(y) \leftarrow \psi_{\theta}(y) = \varepsilon \log v_{\theta}(y) + \frac{\|y\|^2}{2}.$$

Our result can be interpreted as the bound on the quality of approximate solution  $\gamma_{\theta, w}$  (3) recovered from the approximate solution to the dual problem (4). It can be directly proved using the original  $(\phi, \psi)$  notation of the dual problem, but we use  $(u_w, v_{\theta})$  instead as with this change of variables the form of the recovered plan  $\gamma_{\theta, w}$  is more interpretable ( $u_w$  defines the first marginal,  $v_{\theta}$  – conditionals).

Instead of optimizing (6) to get  $\gamma_{\theta, w}$ , we may optimize the upper bound (10) which is more tractable. Indeed, (10) is a sum of the expectations w.r.t. the probability measures  $p, q$ . We can obtain Monte-Carlo estimation of (10) from random samples and optimize it with stochastic gradient descent procedure w.r.t.  $(\theta, w)$ . The main **challenge** here is the computation of the variable  $c_{\theta}$  and term  $\|u_w\|_1$ . Below we propose a smart parametrization by which both variables can be derived analytically.

## 4.2 Parameterization and the Optimization Procedure

**Paramaterization.** Recall that  $u_w$  parametrizes the density of the marginal  $\gamma_x^*$  which is unnormalized. Setting  $x = 0$  in equation (7), we get  $\gamma^*(y|x=0) \propto v^*(y)$  which means that  $v^*$  also corresponds to unnormalized density of the measure. These motivate us to use the unnormalized Gaussian mixture parametrization for the potential  $v_{\theta}(y)$  and measure  $u_w(x)$ :

$$v_{\theta}(y) = \sum_{k=1}^K \alpha_k \mathcal{N}(y|r_k, \varepsilon S_k); \quad u_w(x) = \sum_{l=1}^L \beta_l \mathcal{N}(x|\mu_l, \varepsilon \Sigma_l). \quad (11)$$

Here  $\theta \stackrel{\text{def}}{=} \{\alpha_k, r_k, S_k\}_{k=1}^K$ ,  $w \stackrel{\text{def}}{=} \{\beta_l, \mu_l, \Sigma_l\}_{l=1}^L$  with  $\alpha_k, \beta_l \geq 0$ ,  $r_k, \mu_l \in \mathbb{R}^d$  and  $0 \prec S_k, \Sigma_l \in \mathbb{R}^{d \times d}$ . The covariance matrices are scaled by  $\varepsilon$  just for convenience.

For this type of parametrization, it holds that  $\|u_w\|_1 = \sum_{l=1}^L \beta_l$ . Moreover, there exist closed-form expressions for the normalization constant  $c_{\theta}(x)$  and conditional plan  $\gamma_{\theta}(y|x)$ , see [39, Proposition 3.2]. Specifically, define  $r_k(x) \stackrel{\text{def}}{=} r_k + S_k x$  and  $\tilde{\alpha}_k(x) \stackrel{\text{def}}{=} \alpha_k \exp\left\{\frac{x^T S_k x + 2r_k^T x}{2\varepsilon}\right\}$ . It holds that

$$c_{\theta}(x) = \sum_{k=1}^K \tilde{\alpha}_k(x); \quad \gamma_{\theta}(y|x) = \frac{1}{c_{\theta}(x)} \sum_{k=1}^K \tilde{\alpha}_k(x) \mathcal{N}(y|r_k(x), \varepsilon S_k). \quad (12)$$

Using this result and (11), we get the expression for  $\gamma_{\theta, w}$ :

$$\gamma_{\theta,w}(x,y) = u_w(x) \cdot \gamma_\theta(y|x) = \underbrace{\sum_{l=1}^L \beta_l \mathcal{N}(x|\mu_l, \varepsilon \Sigma_l)}_{u_w(x)} \cdot \underbrace{\frac{\sum_{k=1}^K \tilde{\alpha}_k(x) \mathcal{N}(y|r_k(x), \varepsilon S_k)}{\sum_{k=1}^K \tilde{\alpha}_k(x)}}_{\gamma_\theta(y|x)}. \quad (13)$$

**Training.** We recall that the measures  $p, q$  are accessible only by a number of empirical samples (see the learning setup in §2). Thus, given samples  $\{x_1, \dots, x_N\}$  and  $\{y_1, \dots, y_M\}$ , we optimize the empirical analogue of (10):

$$\widehat{\mathcal{L}}(\theta, w) \stackrel{\text{def}}{=} \frac{1}{N} \sum_{i=1}^N \bar{f}_1(-\varepsilon \log \frac{u_w(x_i)}{c_\theta(x_i)} - \frac{\|x_i\|^2}{2}) + \frac{1}{M} \sum_{j=1}^M \bar{f}_2(-\varepsilon \log v_\theta(y_j) - \frac{\|y_j\|^2}{2}) + \varepsilon \|u_w\|_1 \quad (14)$$

using minibatch gradient descent procedure w.r.t. parameters  $(\theta, w)$ . In the parametrization of  $v_\theta$  and  $u_w$  (11), we utilize the diagonal matrices  $S_k, \Sigma_l$ . This allows for decreasing the number of learnable parameters in  $\theta$  and speeding up the computation of  $S_k^{-1}, \Sigma_l^{-1}$ .

**Inference.** Sampling from the conditional and marginal measures  $\gamma_{\theta,w}(y|x) \approx \gamma^*(y|x)$ ,  $u_w \approx \gamma_x^*$  is easy and lightweight since they are explicitly parametrized as Gaussian mixtures, see (12), (11).

### 4.3 Connection to Related Prior Works

The idea of using Gaussian Mixture parametrization for dual potentials in EOT-related tasks first appeared in the EOT/SB benchmark [29]. There it was used to obtain the benchmark pairs of probability measures with the known EOT solution between them. In [39], the authors utilized this type of parametrization to obtain a light solver (**LightSB**) for the **balanced** EOT.

Our solver for **unbalanced** EOT (10) subsumes their solver for balanced EOT as well as one problem subsumes the other for the special case of divergences, see the remark in §2. Let  $f_1, f_2$  be convex indicators of  $\{1\}$ . Then  $\bar{f}_1(t) = t$  and  $\bar{f}_2(t) = t$  and objective (10) becomes

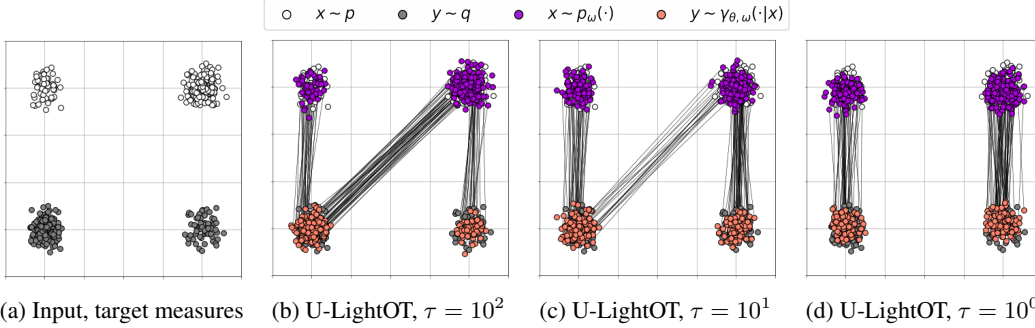
$$\begin{aligned} \mathcal{L}(\theta, w) &= \int_{\mathbb{R}^d} (-\varepsilon \log \frac{u_w(x)}{c_\theta(x)} - \frac{\|x\|^2}{2}) p(x) dx + \int_{\mathbb{R}^d} (-\varepsilon \log v_\theta(y) - \frac{\|y\|^2}{2}) q(y) dy + \varepsilon \|u_w\|_1 = \\ &= -\varepsilon \left( \int_{\mathbb{R}^d} \log \frac{u_w(x)}{c_\theta(x)} p(x) dx + \int_{\mathbb{R}^d} \log v_\theta(y) q(y) dy - \|u_w\|_1 \right) - \underbrace{\int_{\mathbb{R}^d} \frac{\|x\|^2}{2} p(x) dx - \int_{\mathbb{R}^d} \frac{\|y\|^2}{2} q(y) dy}_{\stackrel{\text{def}}{=} C(p,q)} = \\ &= \varepsilon \left( \int_{\mathbb{R}^d} \log c_\theta(x) p(x) dx - \int_{\mathbb{R}^d} \log v_\theta(y) q(y) dy \right) - \quad (15) \\ &= \varepsilon \int_{\mathbb{R}^d} \log u_w(x) p(x) dx + \varepsilon \|u_w\|_1 - C(p, q). \quad (16) \end{aligned}$$

Here line (15) depends exclusively on  $\theta$  and exactly coincides with the LightSB's objective, see [39, Proposition 8]. At the same time, line (16) depends only on  $\omega$ , and its minimum is attained when  $u_w = p$ . Thus, this part is not actually needed in the balanced case, see [39, Appendix C].

### 4.4 Generalization Bounds and Universal Approximation Property

Theoretically, to recover the UEOT plan  $\gamma^*$ , one needs to solve the problem  $\mathcal{L}(\theta, \omega) \rightarrow \min_{\theta, \omega}$  as stated in our Theorem 4.1. In practice, the measures  $p$  and  $q$  are accessible via empirical samples  $\{x_1, \dots, x_N\}$  and  $\{y_1, \dots, y_M\}$ , thus, one needs to optimize the empirical counterpart  $\widehat{\mathcal{L}}(\theta, \omega)$  of  $\mathcal{L}(\theta, \omega)$ , see (14). Besides, the available potentials  $u_w, v_\theta$  over which one optimizes the objective come from the restricted class of functions. Specifically, we consider unnormalized Gaussian mixtures  $u_w, v_\theta$  with  $K$  and  $L$  components respectively. Thus, one may naturally wonder: **how close is the recovered plan  $\gamma_{\widehat{\theta}, \widehat{\omega}}$  to the UEOT plan  $\gamma^*$**  given that  $(\widehat{\theta}, \widehat{\omega}) = \arg \min_{\theta, \omega} \widehat{\mathcal{L}}(\theta, \omega)$ ? To address this question, we study the *generalization error*  $\mathbb{E} D_{\text{KL}}(\gamma^* \parallel \gamma_{\widehat{\theta}, \widehat{\omega}})$ , i.e., the expectation of  $D_{\text{KL}}$  between  $\gamma^*$  and  $\gamma_{\widehat{\theta}, \widehat{\omega}}$  taken w.r.t. the random realization of the train datasets  $X \sim p, Y \sim q$ .

Let  $(\bar{\theta}, \bar{\omega}) = \arg \min_{(\theta, \omega) \in \Theta \times \Omega} \mathcal{L}(\theta, \omega)$  denote the best approximators of  $\mathcal{L}(\theta, \omega)$  in the admissible class. From Theorem 4.1 it follows that that the generalization error  $\mathbb{E} D_{\text{KL}}(\gamma^* \parallel \gamma_{\bar{\theta}, \bar{\omega}})$  can be bounded



(a) Input, target measures (b) U-LightOT,  $\tau = 10^2$  (c) U-LightOT,  $\tau = 10^1$  (d) U-LightOT,  $\tau = 10^0$   
 Figure 1: Conditional plans  $\gamma_{\theta, \omega}(y|x)$  learned by our solver in *Gaussians Mixture* experiment with unbalancedness parameter  $\tau \in [10^0, 10^1, 10^2]$ . Here  $p_\omega$  denotes the normalized first marginal  $u_\omega$ , i.e.,  $p_\omega = u_\omega / \|u_\omega\|_1$ .

by  $\mathbb{E}[\mathcal{L}(\hat{\theta}, \hat{\omega}) - \mathcal{L}^*]$ . The latter can be decomposed into the estimation and approximation errors:

$$\mathbb{E}[\mathcal{L}(\hat{\theta}, \hat{\omega}) - \mathcal{L}^*] = \mathbb{E}[\mathcal{L}(\hat{\theta}, \hat{\omega}) - \mathcal{L}(\bar{\theta}, \bar{\omega})] + \mathbb{E}[\mathcal{L}(\bar{\theta}, \bar{\omega}) - \mathcal{L}^*] = \underbrace{\mathbb{E}[\mathcal{L}(\hat{\theta}, \hat{\omega}) - \mathcal{L}(\bar{\theta}, \bar{\omega})]}_{\text{Estimation error}} + \underbrace{[\mathcal{L}(\bar{\theta}, \bar{\omega}) - \mathcal{L}^*]}_{\text{Approximation error}}. \quad (17)$$

We establish the quantitative bound for the estimation error in the proposition below.

**Proposition 4.2** (Bound for the estimation error). *Let  $p, q$  be compactly supported and assume that  $\bar{f}_1, \bar{f}_2$  are Lipschitz. Assume that the considered parametric classes  $\Theta, \Omega (\ni (\theta, \omega))$  consist of unnormalized Gaussian mixtures with  $K$  and  $L$  components respectively with bounded means  $\|r_k\|, \|\mu_l\| \leq R$  (for some  $R > 0$ ), covariances  $sI \preceq S_k, \Sigma_l \preceq SI$  (for some  $0 < s \leq S$ ) and weights  $a \leq \alpha_k, \beta_l \leq A$  (for some  $0 < a \leq A$ ). Then the following holds:*

$$\mathbb{E}[\mathcal{L}(\hat{\theta}, \hat{\omega}) - \mathcal{L}(\bar{\theta}, \bar{\omega})] \leq O\left(\frac{1}{\sqrt{N}}\right) + O\left(\frac{1}{\sqrt{M}}\right),$$

where  $O(\cdot)$  hides the constants depending only on  $K, L, R, s, S, a, A, p, q, \varepsilon$  but not on sizes  $M, N$ .

This proposition allows us to conclude that the estimation error converges to zero (when  $N$  and  $M$  tend to infinity) at the usual Monte-Carlo rate. It remains to clarify the question: *can we make the approximation error arbitrarily small?* We answer this question positively in our Theorem below.

**Theorem 4.3** (Gaussian mixture parameterization for the variables provides the universal approximation of UEOT plans). *Let  $p$  and  $q$  be compactly supported. Then for all  $\delta > 0$  there exist Gaussian mixtures  $v_\theta, u_\omega$  (11) with **scalar** covariances  $S_k = \lambda_k I_d > 0, \Sigma_l = \zeta_l I_d > 0$  of their components that satisfy the inequality  $D_{KL}(\gamma^* || \gamma_{\theta, \omega}) \leq \varepsilon^{-1}(\mathcal{L}(\theta, \omega) - \mathcal{L}^*) < \delta$ .*

**In summary**, results of this section show that one can make the generalization error *arbitrarily small* given a sufficiently large amount of samples and components in the Gaussian parametrization. It means that theoretically our solver can recover the UEOT plan arbitrarily well.

## 5 Experiments

In this section, we test our U-LightOT solver on several setups from the related works. The code is written using PyTorch framework and will be made public. The experiments are issued in the convenient form of \*.ipynb notebooks. Each experiment requires several minutes of training on CPU with 4 cores. Technical *training details* are given in Appendix B.

### 5.1 Example with the Mixture of Gaussians

We provide an illustrative 'Gaussians Mixture' example in 2D to demonstrate the ability of our solver to deal with the imbalance of classes in the source and target measures. We follow the experimental setup proposed in [16, Figure 2] and define the probability measures  $p, q$  as follows (Fig. 3a):

$$p(x) = \frac{1}{4} \mathcal{N}(x|(-2, 3), 0.1 \cdot I_2) + \frac{3}{4} \mathcal{N}(x|(1, 3), 0.1 \cdot I_2),$$

$$q(y) = \frac{3}{4} \mathcal{N}(y|(-2, 0), 0.1 \cdot I_2) + \frac{1}{4} \mathcal{N}(y|(1, 0), 0.1 \cdot I_2).$$

Experiment	OT-FM [16]	[39, LightSB] or [30, LightSBM]	[16, UOT-FM]	UOT-SD [9]	UOT-GAN [68]	U-LightOT (ours)
<i>Young</i> → <i>Adult</i>	60.71	87.11	<u>87.72</u>	46.02	85.95	<b>94.63</b>
<i>Adult</i> → <i>Young</i>	56.75	76.68	81.34	54.27	<u>88.37</u>	<b>94.36</b>
<i>Man</i> → <i>Woman</i>	73.82	81.33	<u>87.35</u>	72.53	83.79	<b>92.85</b>
<i>Woman</i> → <i>Man</i>	77.56	83.29	<u>88.20</u>	75.03	<u>89.32</u>	<b>95.13</b>

Table 2: Comparison of accuracies of keeping the attributes of the source images.

The best results are in **bold**, second best are underlined.

We test our U-LightOT solver with *scaled*  $D_{\text{KL}}$  divergences, i.e.,  $f_1(t), f_2(t)$  are defined by  $\tau \cdot f_{\text{KL}}(t) = \tau(t \log(t) - t + 1)$  where  $\tau > 0$ . We provide the learned plans for  $\tau \in [1, 10^2, 10^3]$ . The results show that parameter  $\tau$  can be used to control the level of unbalancedness of the learned plans. For  $\tau = 1$ , our U-LightOT solver truly learns the UEOT plans, see Fig. 3d. When  $\tau$  increases, the solver fails to transport the mass from the input Gaussians to the closest target ones. Actually, for  $\tau = 10^3$ , our solutions are similar to the solutions of the balanced solver [39, LightSB] which approximates EOT plans between the measures. Hereafter, we treat  $\tau$  as an *unbalancedness* parameter. In Appendix C, we test the performance of our solver with  $D_{\chi^2}$  divergence.

*Remark.* We conduct all experiments here with the entropy regularization parameter  $\varepsilon = 0.05$ . The parameter  $\varepsilon$  is responsible for the stochasticity of the learned transport  $\gamma_\theta(\cdot|x)$ . Since we are mostly interested in the correct transport of the mass (controlled by  $f_1, f_2$ ) rather than the stochasticity, we do not pay much attention to  $\varepsilon$  throughout the paper.

## 5.2 Unpaired Image-to-Image Translation

Another popular testbed which is usually considered in OT/EOT papers is the unpaired image-to-image translation [69] task. Since our solver uses the parametrization based on Gaussian mixture, it may be hard to apply U-LightOT for learning translation directly in the image space. Fortunately, nowadays it is common to use autoencoders [57] for more efficient translation. We follow the setup of [39, Section 5.4] and use pre-trained ALAE autoencoder [53] for  $1024 \times 1024$  FFHQ dataset [33] of human faces. We consider different subsets of FFHQ dataset (*Adult, Young, Man, Woman*) and all variants of translations between them: *Adult*↔*Young* and *Woman*↔*Man*.

The main challenge of the described translations is the **imbalance** of classes in the images from source and target subsets, see Table 3. Let us consider in more detail *Adult*→*Young* translation. In the FFHQ dataset, the amount of *adult women* significantly outnumbers the *adult men*, while the amount of *young women* is smaller than that of *young men*. Thus, balanced OT/EOT solvers are expected to translate some of the *young woman* representatives to the *adult man* ones. At the same time, solvers based on unbalanced transport are supposed to alleviate this issue.

Class	Man	Woman
<i>Young</i>	15K	23K
<i>Adult</i>	7K	3.5K

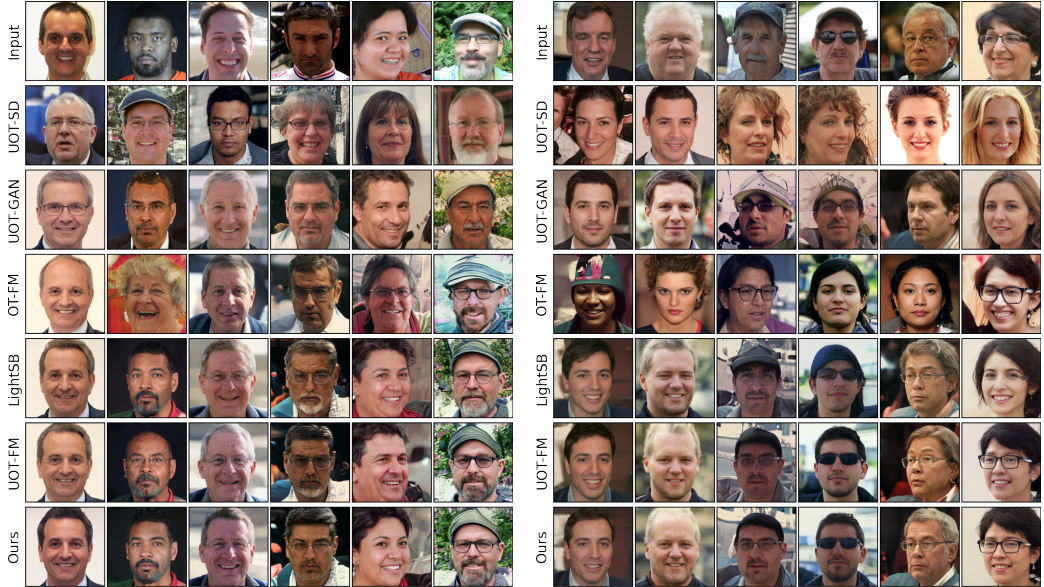
Table 3: Number of *train* FFHQ images for each subset.

**Baselines.** We perform a comparison with the recent procedure [16, UOT-FM] which considers roughly the same setup and demonstrates good performance. This method interpolates the results of unbalanced discrete OT to the continuous setup using the flow matching [42]. For completeness, we include the comparison with LightSB and balanced optimal transport-based flow matching (OT-FM) [42] to demonstrate the issues of the balanced solvers. We also considered neural network based solvers such as UOT-SD[9] and UOT-GAN[68].

**Metrics.** We aim to assess the ability of the solvers to perform the translation of latent codes keeping the class of the input images unchanged, e.g., keeping the gender in *Adult*→*Young* translation. Thus, we train a 99% MLP classifier on the latent codes of images of different classes and compute the accuracy between the classes of the source images and those of the generated ones.

**Results.** Our evaluation shows that U-LightOT solver can effectively solve translation tasks in high dimensions ( $d = 512$ ) and outperforms its alternatives in dealing with class imbalance issues. In Table 2, we quantitatively demonstrate this effect. Namely, we show that our solver achieves the best accuracy of keeping the class of source images. Qualitative examples are given in Fig. 2. In Appendix E, we give *additional qualitative results*. Additionally, in Appendix C, we perform the *ablation study* of our solver focusing on the selection of parameters  $\tau, \varepsilon$ .





(a) *Young*  $\rightarrow$  *Adult*

(b) *Adult*  $\rightarrow$  *Young*



(c) *Man*  $\rightarrow$  *Woman*

(d) *Woman*  $\rightarrow$  *Man*

Figure 2: Unpaired translation with LightSB, OT-FM, UOT-FM and our U-LightOT solver applied in the latent space of ALAE for FFHQ images ( $1024 \times 1024$ ).

## 6 Discussion

**Potential impact.** Our light and unbalanced solver has a lot of advantages in comparison with the other existing UEOT solvers. First, it does not require complex max-min optimization. Second, it provides the closed form of the conditional measures  $\gamma_{\theta, \omega}(y|x) \approx \gamma^*(y|x)$  of the UEOT plan. Moreover, it allows for sampling both from the conditional measure  $\gamma_{\theta, \omega}(y|x)$  and marginal measure  $u_w(x) \approx \gamma_x^*(x)$ . Besides, the decisive superiority of our lightweight and unbalanced solver is its simplicity and convenience of use. Indeed, it has a straightforward and non-minimax optimization objective and avoids heavy neural parametrization. As a result, our lightweight and unbalanced solver converges in minutes on CPU. We expect that these advantages could boost the usage of our solver as a standard and easy baseline for UEOT task with applications in different spheres.

The limitations and broader impact of our solver are discussed in Appendix D.

## References

- [1] R. Agrawal and T. Horel. Optimal bounds between f-divergences and integral probability metrics. *Journal of Machine Learning Research*, 22(128):1–59, 2021.
- [2] M. Arjovsky, S. Chintala, and L. Bottou. Wasserstein generative adversarial networks. In *International conference on machine learning*, pages 214–223. PMLR, 2017.
- [3] A. Asadulaev, A. Korotin, V. Egiazarian, and E. Burnaev. Neural optimal transport with general cost functionals. In *The Twelfth International Conference on Learning Representations*, 2024.
- [4] Y. Balaji, R. Chellappa, and S. Feizi. Robust optimal transport with applications in generative modeling and domain adaptation. *Advances in Neural Information Processing Systems*, 33: 12934–12944, 2020.
- [5] C. Bunne, S. G. Stark, G. Gut, J. S. Del Castillo, M. Levesque, K.-V. Lehmann, L. Pelkmans, A. Krause, and G. Rätsch. Learning single-cell perturbation responses using neural optimal transport. *Nature Methods*, 20(11):1759–1768, 2023.
- [6] L. Chapel, R. Flamary, H. Wu, C. Févotte, and G. Gasso. Unbalanced optimal transport through non-negative penalized linear regression. *Advances in Neural Information Processing Systems*, 34:23270–23282, 2021.
- [7] T. Chen, G.-H. Liu, and E. Theodorou. Likelihood training of schrödinger bridge using forward-backward sdes theory. In *International Conference on Learning Representations*, 2021.
- [8] L. Chizat. *Unbalanced optimal transport: Models, numerical methods, applications*. PhD thesis, Université Paris sciences et lettres, 2017.
- [9] J. Choi, J. Choi, and M. Kang. Generative modeling through the semi-dual formulation of unbalanced optimal transport. *arXiv preprint arXiv:2305.14777*, 2023.
- [10] M. Cuturi. Sinkhorn distances: Lightspeed computation of optimal transport. In *Advances in neural information processing systems*, pages 2292–2300, 2013.
- [11] M. Daniels, T. Maunu, and P. Hand. Score-based generative neural networks for large-scale optimal transport. *Advances in neural information processing systems*, 34:12955–12965, 2021.
- [12] Q. Dao, B. Ta, T. Pham, and A. Tran. Robust diffusion gan using semi-unbalanced optimal transport. *arXiv preprint arXiv:2311.17101*, 2023.
- [13] V. De Bortoli, J. Thornton, J. Heng, and A. Doucet. Diffusion schrödinger bridge with applications to score-based generative modeling. *Advances in Neural Information Processing Systems*, 34:17695–17709, 2021.
- [14] N. Deb, P. Ghosal, and B. Sen. Rates of estimation of optimal transport maps using plug-in estimators via barycentric projections. *Advances in Neural Information Processing Systems*, 34: 29736–29753, 2021.
- [15] P. Dvurechenskii, D. Dvinskikh, A. Gasnikov, C. Uribe, and A. Nedich. Decentralize and randomize: Faster algorithm for Wasserstein barycenters. In *Advances in Neural Information Processing Systems*, pages 10760–10770, 2018.
- [16] L. Eyring, D. Klein, T. Uscidda, G. Palla, N. Kilbertus, Z. Akata, and F. Theis. Unbalancedness in neural monge maps improves unpaired domain translation. In *The Twelfth International Conference on Learning Representations*, 2024.
- [17] J. Fan, A. Taghvaei, and Y. Chen. Scalable computations of Wasserstein barycenter via input convex neural networks. *arXiv preprint arXiv:2007.04462*, 2020.
- [18] J. Fan, S. Liu, S. Ma, H.-M. Zhou, and Y. Chen. Neural monge map estimation and its applications. *Transactions on Machine Learning Research*, 2023. ISSN 2835-8856. URL <https://openreview.net/forum?id=2mZS1Qscj3>. Featured Certification.

- [19] K. Fatras, Y. Zine, R. Flamary, R. Gribonval, and N. Courty. Learning with minibatch wasserstein: asymptotic and gradient properties. In *AISTATS 2020-23rd International Conference on Artificial Intelligence and Statistics*, volume 108, pages 1–20, 2020.
- [20] K. Fatras, T. Séjourné, R. Flamary, and N. Courty. Unbalanced minibatch optimal transport; applications to domain adaptation. In *International Conference on Machine Learning*, pages 3186–3197. PMLR, 2021.
- [21] R. Flamary, N. Courty, A. Gramfort, M. Z. Alaya, A. Boisbunon, S. Chambon, L. Chapel, A. Corenflos, K. Fatras, N. Fournier, et al. Pot: Python optimal transport. *The Journal of Machine Learning Research*, 22(1):3571–3578, 2021.
- [22] M. Gazdieva, L. Rout, A. Korotin, A. Kravchenko, A. Filippov, and E. Burnaev. An optimal transport perspective on unpaired image super-resolution. *arXiv preprint arXiv:2202.01116*, 2022.
- [23] M. Gazdieva, A. Korotin, D. Selikhanovych, and E. Burnaev. Extremal domain translation with neural optimal transport. In *Advances in Neural Information Processing Systems*, volume 36, 2023.
- [24] A. Genevay. *Entropy-Regularized Optimal Transport for Machine Learning*. Theses, PSL University, Mar. 2019. URL <https://theses.hal.science/tel-02319318>.
- [25] A. Genevay, G. Peyré, and M. Cuturi. Learning generative models with sinkhorn divergences. In *International Conference on Artificial Intelligence and Statistics*, pages 1608–1617. PMLR, 2018.
- [26] N. Gozlan, C. Roberto, P.-M. Samson, and P. Tetali. Kantorovich duality for general transport costs and applications. *Journal of Functional Analysis*, 273(11):3327–3405, 2017.
- [27] I. Gulrajani, F. Ahmed, M. Arjovsky, V. Dumoulin, and A. C. Courville. Improved training of Wasserstein GANs. In *Advances in Neural Information Processing Systems*, pages 5767–5777, 2017.
- [28] N. Gushchin, A. Kolesov, A. Korotin, D. Vetrov, and E. Burnaev. Entropic neural optimal transport via diffusion processes. In *Advances in Neural Information Processing Systems*, 2023.
- [29] N. Gushchin, A. Kolesov, P. Mokrov, P. Karpikova, A. Spiridonov, E. Burnaev, and A. Korotin. Building the bridge of schrödinger: A continuous entropic optimal transport benchmark. *arXiv preprint arXiv:2306.10161*, 2023.
- [30] N. Gushchin, S. Kholkin, E. Burnaev, and A. Korotin. Light and optimal schrödinger bridge matching. In *arXiv preprint arXiv:2402.03207*, 2024.
- [31] J.-C. Hütter and P. Rigollet. Minimax estimation of smooth optimal transport maps. 2021.
- [32] H. Janati, B. Muzellec, G. Peyré, and M. Cuturi. Entropic optimal transport between unbalanced gaussian measures has a closed form. *Advances in neural information processing systems*, 33: 10468–10479, 2020.
- [33] T. Karras, S. Laine, and T. Aila. A style-based generator architecture for generative adversarial networks. In *Proceedings of the IEEE/CVF conference on computer vision and pattern recognition*, pages 4401–4410, 2019.
- [34] D. Klein, T. Uscidda, F. Theis, and M. Cuturi. Generative entropic neural optimal transport to map within and across spaces. *arXiv preprint arXiv:2310.09254*, 2023.
- [35] A. Korotin, L. Li, A. Genevay, J. M. Solomon, A. Filippov, and E. Burnaev. Do neural optimal transport solvers work? a continuous wasserstein-2 benchmark. *Advances in Neural Information Processing Systems*, 34:14593–14605, 2021.
- [36] A. Korotin, L. Li, J. Solomon, and E. Burnaev. Continuous wasserstein-2 barycenter estimation without minimax optimization. In *International Conference on Learning Representations*, 2021. URL <https://openreview.net/forum?id=3tFAs5E-Pe>.

- [37] A. Korotin, A. Kolesov, and E. Burnaev. Kantorovich strikes back! wasserstein gans are not optimal transport? In *Thirty-sixth Conference on Neural Information Processing Systems Datasets and Benchmarks Track*, 2022.
- [38] A. Korotin, D. Selikhanovych, and E. Burnaev. Kernel neural optimal transport. In *International Conference on Learning Representations*, 2023. URL [https://openreview.net/forum?id=Zuc\\_MHtUma4](https://openreview.net/forum?id=Zuc_MHtUma4).
- [39] A. Korotin, N. Gushchin, and E. Burnaev. Light schrödinger bridge. In *The Twelfth International Conference on Learning Representations*, 2024.
- [40] T. Koshizuka and I. Sato. Neural lagrangian schrödinger bridge: Diffusion modeling for population dynamics. In *The Eleventh International Conference on Learning Representations*, 2022.
- [41] M. Liero, A. Mielke, and G. Savaré. Optimal entropy-transport problems and a new hellinger-kantorovich distance between positive measures. *Inventiones mathematicae*, 211(3):969–1117, 2018.
- [42] Y. Lipman, R. T. Chen, H. Ben-Hamu, M. Nickel, and M. Le. Flow matching for generative modeling. *arXiv preprint arXiv:2210.02747*, 2022.
- [43] F. Lübeck, C. Bunne, G. Gut, J. S. del Castillo, L. Pelkmans, and D. Alvarez-Melis. Neural unbalanced optimal transport via cycle-consistent semi-couplings. *arXiv preprint arXiv:2209.15621*, 2022.
- [44] M. Lucic, K. Kurach, M. Michalski, S. Gelly, and O. Bousquet. Are GANs created equal? a large-scale study. In *Advances in neural information processing systems*, pages 700–709, 2018.
- [45] A. Makkuva, A. Taghvaei, S. Oh, and J. Lee. Optimal transport mapping via input convex neural networks. In *International Conference on Machine Learning*, pages 6672–6681. PMLR, 2020.
- [46] T. Manole, S. Balakrishnan, J. Niles-Weed, and L. Wasserman. Plugin estimation of smooth optimal transport maps. *arXiv preprint arXiv:2107.12364*, 2021.
- [47] M. Mohri, A. Rostamizadeh, and A. Talwalkar. *Foundations of machine learning*. MIT press, 2018.
- [48] P. Mokrov, A. Korotin, and E. Burnaev. Energy-guided entropic neural optimal transport. In *The Twelfth International Conference on Learning Representations*, 2024.
- [49] Q. M. Nguyen, H. H. Nguyen, Y. Zhou, and L. M. Nguyen. On unbalanced optimal transport: Gradient methods, sparsity and approximation error. *arXiv preprint arXiv:2202.03618*, 2022.
- [50] T. T. Nguyen, H. D. Nguyen, F. Chamroukhi, and G. J. McLachlan. Approximation by finite mixtures of continuous density functions that vanish at infinity. *Cogent Mathematics & Statistics*, 7(1):1750861, 2020.
- [51] G. Peyré, M. Cuturi, et al. Computational optimal transport. *Foundations and Trends® in Machine Learning*, 11(5-6):355–607, 2019.
- [52] K. Pham, K. Le, N. Ho, T. Pham, and H. Bui. On unbalanced optimal transport: An analysis of sinkhorn algorithm. In *International Conference on Machine Learning*, pages 7673–7682. PMLR, 2020.
- [53] S. Pidhorskyi, D. A. Adjeroh, and G. Doretto. Adversarial latent autoencoders. In *Proceedings of the IEEE/CVF Conference on Computer Vision and Pattern Recognition*, pages 14104–14113, 2020.
- [54] A.-A. Pooladian and J. Niles-Weed. Entropic estimation of optimal transport maps. *arXiv preprint arXiv:2109.12004*, 2021.
- [55] P. Rigollet and A. J. Stromme. On the sample complexity of entropic optimal transport. *arXiv preprint arXiv:2206.13472*, 2022.

- [56] R. Rockafellar. Duality and stability in extremum problems involving convex functions. *Pacific Journal of Mathematics*, 21(1):167–187, 1967.
- [57] R. Rombach, A. Blattmann, D. Lorenz, P. Esser, and B. Ommer. High-resolution image synthesis with latent diffusion models. In *Proceedings of the IEEE/CVF conference on computer vision and pattern recognition*, pages 10684–10695, 2022.
- [58] L. Rout, A. Korotin, and E. Burnaev. Generative modeling with optimal transport maps. In *International Conference on Learning Representations*, 2022.
- [59] V. Seguy, B. B. Damodaran, R. Flamary, N. Courty, A. Rolet, and M. Blondel. Large scale optimal transport and mapping estimation. In *International Conference on Learning Representations*, 2018.
- [60] T. Séjourné, G. Peyré, and F.-X. Vialard. Unbalanced optimal transport, from theory to numerics. *arXiv preprint arXiv:2211.08775*, 2022.
- [61] S. Shalev-Shwartz and S. Ben-David. *Understanding machine learning: From theory to algorithms*. Cambridge university press, 2014.
- [62] A. Taghvaei and A. Jalali. 2-Wasserstein approximation via restricted convex potentials with application to improved training for GANs. *arXiv preprint arXiv:1902.07197*, 2019.
- [63] A. Tong, J. Huang, G. Wolf, D. Van Dijk, and S. Krishnaswamy. Trajectorynet: A dynamic optimal transport network for modeling cellular dynamics. In *International conference on machine learning*, pages 9526–9536. PMLR, 2020.
- [64] F. Vargas, P. Thodoroff, A. Lamacraft, and N. Lawrence. Solving schrödinger bridges via maximum likelihood. *Entropy*, 23(9):1134, 2021.
- [65] G. Wang, Y. Jiao, Q. Xu, Y. Wang, and C. Yang. Deep generative learning via schrödinger bridge. In *International Conference on Machine Learning*, pages 10794–10804. PMLR, 2021.
- [66] Y. Xie, M. Chen, H. Jiang, T. Zhao, and H. Zha. On scalable and efficient computation of large scale optimal transport. volume 97 of *Proceedings of Machine Learning Research*, pages 6882–6892, Long Beach, California, USA, 09–15 Jun 2019. PMLR. URL <http://proceedings.mlr.press/v97/xie19a.html>.
- [67] Y. Xie, Y. Luo, and X. Huo. An accelerated stochastic algorithm for solving the optimal transport problem. *arXiv preprint arXiv:2203.00813*, 2022.
- [68] K. D. Yang and C. Uhler. Scalable unbalanced optimal transport using generative adversarial networks. In *International Conference on Learning Representations*, 2018.
- [69] J.-Y. Zhu, R. Zhang, D. Pathak, T. Darrell, A. A. Efros, O. Wang, and E. Shechtman. Toward multimodal image-to-image translation. *Advances in neural information processing systems*, 30, 2017.

## A Proofs

### A.1 Proof of Theorem 4.1

*Proof.* To begin with, we derive the useful property of the optimal UEOT plans. We recall that  $\phi^*$  and  $\psi^*$  are the minimizers of dual form (4), i.e.,  $(\phi^*, \psi^*) \in \arg \min_{(\phi, \psi)} \mathcal{J}(\phi, \psi)$  where

$$\mathcal{J}(\phi, \psi) \stackrel{\text{def}}{=} \varepsilon \int_{\mathbb{R}^d} \int_{\mathbb{R}^d} \exp\left\{\frac{1}{\varepsilon}(\phi(x) + \psi(y) - \frac{\|x-y\|^2}{2})\right\} dx dy + \int_{\mathbb{R}^d} \bar{f}_1(-\phi(x)) p(x) dx + \int_{\mathbb{R}^d} \bar{f}_2(-\psi(y)) q(y) dy. \quad (18)$$

Then, by the first order optimality condition  $\frac{d}{d\phi} \mathcal{J}(\phi, \psi)|_{\phi=\phi^*} = 0$  and  $\frac{d}{d\psi} \mathcal{J}(\phi, \psi)|_{\psi=\psi^*} = 0$ . It means that

$$\frac{d}{d\phi} \mathcal{J}(\phi, \psi)|_{\phi=\phi^*}(x) = \varepsilon^{-1} \int_{\mathbb{R}^d} \exp\{\varepsilon^{-1}(\phi^*(x) + \psi^*(y) - \|x-y\|^2/2)\} dy - \nabla \bar{f}_1(-\phi^*(x)) p(x) = 0 \implies \nabla \bar{f}_1(-\phi^*(x)) = \frac{\gamma_x^*(x)}{p(x)} \quad (19)$$

holds for all  $x$ , s.t.  $p(x) > 0$ . Analogously, we get that  $\nabla \bar{f}_2(-\psi^*(y)) = \frac{\gamma_y^*(y)}{q(y)}$  for all  $y$ , s.t.  $q(y) > 0$ .

For convenience of the further derivations, we consider the change of variables to simplify the expression for  $\mathcal{L}(\theta, \omega)$ . We define  $\phi_{\theta, \omega}(x) \stackrel{\text{def}}{=} \varepsilon \log \frac{u_\omega(x)}{c_\theta(x)} + \frac{\|x\|^2}{2}$  and  $\psi_\theta(y) \stackrel{\text{def}}{=} \varepsilon \log v_\theta(y) + \frac{\|y\|^2}{2}$ . Then

$$\mathcal{L}(\theta, \omega) = \int_{\mathbb{R}^d} \bar{f}_1(-\phi_{\theta, \omega}(x)) p(x) dx + \int_{\mathbb{R}^d} \bar{f}_2(-\psi_\theta(y)) q(y) dy + \varepsilon \|u_\omega\|_1 = \mathcal{J}(\phi_{\theta, \omega}, \psi_\theta).$$

Next, we simplify our main objective:

$$\begin{aligned} \text{D}_{\text{KL}}(\gamma^* \|\gamma_{\theta, \omega}) &= \|\gamma^*\|_1 \left[ \text{D}_{\text{KL}}\left(\frac{\gamma^*}{\|\gamma^*\|_1} \|\frac{\gamma_{\theta, \omega}}{\|\gamma_{\theta, \omega}\|_1}\right) + \frac{\|\gamma_{\theta, \omega}\|_1}{\|\gamma^*\|_1} - 1 - \log \frac{\|\gamma_{\theta, \omega}\|_1}{\|\gamma^*\|_1} \right] = \\ &= \frac{\|\gamma^*\|_1}{\|\gamma^*\|_1} \left( \int_{\mathbb{R}^d \times \mathbb{R}^d} \gamma^*(x, y) \log \gamma^*(x, y) dx dy - \int_{\mathbb{R}^d \times \mathbb{R}^d} \gamma^*(x, y) \log \|\gamma^*\|_1 dx dy - \int_{\mathbb{R}^d \times \mathbb{R}^d} \gamma^*(x, y) \log \gamma_{\theta, \omega}(x, y) dx dy + \right. \\ &\quad \left. \int_{\mathbb{R}^d \times \mathbb{R}^d} \gamma^*(x, y) \log \|\gamma_{\theta, \omega}\|_1 dx dy + \|\gamma_{\theta, \omega}\|_1 - \|\gamma^*\|_1 - \|\gamma^*\|_1 \log \frac{\|\gamma_{\theta, \omega}\|_1}{\|\gamma^*\|_1} \right) = \int_{\mathbb{R}^d \times \mathbb{R}^d} \gamma^*(x, y) \log \gamma^*(x, y) dx dy - \\ &= \frac{\|\gamma^*\|_1}{\|\gamma^*\|_1} \log \|\gamma^*\|_1 - \int_{\mathbb{R}^d \times \mathbb{R}^d} \gamma^*(x, y) \log \gamma_{\theta, \omega}(x, y) dx dy + \frac{\|\gamma^*\|_1}{\|\gamma^*\|_1} \log \|\gamma_{\theta, \omega}\|_1 + \\ &\quad \|\gamma_{\theta, \omega}\|_1 - \|\gamma^*\|_1 - \frac{\|\gamma^*\|_1}{\|\gamma^*\|_1} \log \|\gamma_{\theta, \omega}\|_1 + \\ &= \frac{\|\gamma^*\|_1}{\|\gamma^*\|_1} \log \|\gamma^*\|_1 = \int_{\mathbb{R}^d \times \mathbb{R}^d} \gamma^*(x, y) \log \gamma^*(x, y) dx dy - \\ &\quad \int_{\mathbb{R}^d \times \mathbb{R}^d} \gamma^*(x, y) \log \gamma_{\theta, \omega}(x, y) dx dy + \|\gamma_{\theta, \omega}\|_1 - \|\gamma^*\|_1. \quad (20) \end{aligned}$$

Now we recall that the ground-truth UEOT plan  $\gamma^*(x, y)$  and the optimal dual variables  $\phi^*(x)$ ,  $\psi^*(y)$  are connected via equation (5). Similarly, our parametrized plan  $\gamma_{\theta, \omega}(x, y)$  can be expressed using  $\phi_{\theta, \omega}(x)$ ,  $\psi_\theta(y)$  as  $\gamma_{\theta, \omega}(x, y) = \exp\{\varepsilon^{-1}(\phi_{\theta, \omega}(x) + \psi_\theta(y) - \|x-y\|^2/2)\}$ . Then

$$(20) = \varepsilon^{-1} \int_{\mathbb{R}^d \times \mathbb{R}^d} \gamma^*(x, y) (\phi^*(x) + \psi^*(y) - \|x-y\|^2/2) dx dy -$$

$$\begin{aligned}
& \varepsilon^{-1} \int_{\mathbb{R}^d \times \mathbb{R}^d} \gamma^*(x, y) (\phi_{\theta, \omega}(x) + \psi_{\theta}(y) - \|x-y\|^2/2) dx dy + \|\gamma_{\theta, \omega}\|_1 - \|\gamma^*\|_1 = \\
& \varepsilon^{-1} \int_{\mathbb{R}^d \times \mathbb{R}^d} \gamma^*(x, y) (\phi^*(x) + \psi^*(y) - \phi_{\theta, \omega}(x) - \psi_{\theta}(y)) dx dy + \|\gamma_{\theta, \omega}\|_1 - \|\gamma^*\|_1 = \\
& \varepsilon^{-1} \int_{\mathbb{R}^d} \gamma_x^*(x) (\phi^*(x) - \phi_{\theta, \omega}(x)) dx + \varepsilon^{-1} \int_{\mathbb{R}^d} \gamma_y^*(y) (\psi^*(y) - \psi_{\theta}(y)) dy + \|\gamma_{\theta, \omega}\|_1 - \|\gamma^*\|_1. \quad (21)
\end{aligned}$$

Finally, we derive

$$\begin{aligned}
(21) &= \varepsilon^{-1} \int_{\mathbb{R}^d} \underbrace{\frac{\gamma_x^*(x)}{p(x)}}_{\nabla \bar{f}_1(-\phi^*(x))} (\phi^*(x) - \phi_{\theta, \omega}(x)) p(x) dx + \\
& \varepsilon^{-1} \int_{\mathbb{R}^d} \underbrace{\frac{\gamma_y^*(y)}{q(y)}}_{\nabla \bar{f}_2(-\psi^*(y))} (\psi^*(y) - \psi_{\theta}(y)) q(y) dy + \|\gamma_{\theta, \omega}\|_1 - \|\gamma^*\|_1 = \\
& \varepsilon^{-1} \int_{\mathbb{R}^d} \nabla \bar{f}_1(-\phi^*(x)) (\phi^*(x) - \phi_{\theta, \omega}(x)) p(x) dx + \\
& \varepsilon^{-1} \int_{\mathbb{R}^d} \nabla \bar{f}_2(-\psi^*(y)) (\psi^*(y) - \psi_{\theta}(y)) q(y) dy + \|\gamma_{\theta, \omega}\|_1 - \|\gamma^*\|_1 \leq \quad (22) \\
& \varepsilon^{-1} \int_{\mathbb{R}^d} (\bar{f}_1(-\phi_{\theta, \omega}(x)) - \bar{f}_1(-\phi^*(x))) p(x) dx + \\
& \varepsilon^{-1} \int_{\mathbb{R}^d} (\bar{f}_2(-\psi_{\theta}(y)) - \bar{f}_2(-\psi^*(y))) q(y) dy + \|\gamma_{\theta, \omega}\|_1 - \|\gamma^*\|_1 = \\
& \varepsilon^{-1} \cdot \left( \int_{\mathbb{R}^d} \bar{f}_1(-\phi_{\theta, \omega}(x)) p(x) dx + \int_{\mathbb{R}^d} \bar{f}_2(-\psi_{\theta}(y)) q(y) dy + \varepsilon \|\gamma_{\theta, \omega}\|_1 - \right. \\
& \left. \underbrace{\left( \int_{\mathbb{R}^d} \bar{f}_1(-\phi^*(x)) p(x) dx + \int_{\mathbb{R}^d} \bar{f}_2(-\psi^*(y)) q(y) dy + \varepsilon \|\gamma^*\|_1 \right)}_{\mathcal{L}^* \stackrel{\text{def}}{=} \mathcal{L}^*} \right) = \\
& \varepsilon^{-1} (\mathcal{J}(\phi_{\theta, \omega}, \psi_{\theta}) - \mathcal{L}^*) = \varepsilon^{-1} (\mathcal{L}(\theta, \omega) - \mathcal{L}^*).
\end{aligned}$$

The inequality (22) follows from the convexity of the functions  $\bar{f}_1$  and  $\bar{f}_2$ .  $\square$

## A.2 Proof of Proposition 4.2

We begin with proving the auxiliary theoretical results (Propositions A.1, A.2) which are needed to prove the main proposition of this section.

**Proposition A.1** (Rademacher bound on the estimation error). *It holds that*

$$\mathbb{E}[\mathcal{L}(\hat{\theta}) - \mathcal{L}(\bar{\theta})] \leq 4\mathcal{R}_N(\mathcal{F}_1, p) + 4\mathcal{R}_M(\mathcal{F}_2, q),$$

where  $\mathcal{F}_1 = \{\bar{f}_1(-\phi_{\theta, \omega}) | (\theta, \omega) \in \Theta \times \Omega\}$ ,  $\mathcal{F}_2 = \{\bar{f}_2(-\psi_{\theta}) | \theta \in \Theta\}$  for  $\phi_{\theta, \omega}(x) = \varepsilon \log \frac{u_{\omega}(x)}{c_{\theta}(x)} + \frac{\|x\|^2}{2}$ ,  $\psi_{\theta}(y) = \varepsilon \log v_{\theta}(y) + \frac{\|y\|^2}{2}$ , and  $\mathcal{R}_N(\mathcal{F}_1, p)$ ,  $\mathcal{R}_M(\mathcal{F}_2, q)$  denote the Rademacher complexity [61, §26] of the functional classes  $\mathcal{U}$ ,  $\mathcal{V}$  w.r.t. to the sample sizes  $N$ ,  $M$  of distributions  $p$ ,  $q$ .

*Proof of Proposition A.1.* The derivation of this fact is absolutely analogous to [39, Proposition H.2], [48, Theorem 4] or [62, Theorem 3.4].  $\square$

**Proposition A.2** (Bound on the Rademacher complexity of the considered classes). *Let  $0 < a \leq A$ , let  $0 < u \leq U$ , let  $0 < w \leq W$  and  $V > 0$ . Consider the class of functions*

$$\begin{aligned}
\mathcal{F}_1 &= \left\{ x \mapsto \bar{f}_1(-\varepsilon \log u_w(x) + \varepsilon \log c_{\theta}(x) - \frac{\|x\|^2}{2}) \right\}, \\
\mathcal{F}_2 &= \left\{ y \mapsto \bar{f}_2(-\varepsilon \log v_{\theta}(y) - \frac{\|y\|^2}{2}) \right\} \text{ where}
\end{aligned}$$

$u_\omega(x)$ ,  $v_\theta(y)$ ,  $c_\theta(x)$  belong to the class

$$\mathcal{V} = \left\{ x \mapsto \sum_{k=1}^K \alpha_k \exp(x^T U_k x + v_k^T x + w_k) \text{ with} \right. \quad (23)$$

$$\left. uI \preceq U_k = U_k^T \preceq UI; \|v_k\| \leq V; w \leq w_k \leq W; a \leq \alpha_k \leq A \right\}.$$

Following [39, Proposition H.3], we call the functions of the class  $\mathcal{V}$  as constrained log-sum-exp quadratic functions. We assume that  $\bar{f}_1, \bar{f}_2$  are Lipschitz functions and measures  $p, q$  are compactly supported with the supports lying in a zero-centered ball of a radius  $R > 0$ . Then

$$\mathcal{R}_N(\mathcal{F}_1, p) \leq \frac{C_0}{\sqrt{N}}, \quad \mathcal{R}_M(\mathcal{F}_2, q) \leq \frac{C_1}{\sqrt{M}}$$

where the constants  $C_0, C_1$  **do not depend** on sizes  $N, M$  of the empirical samples from  $p, q$ .

*Proof of Proposition A.2.* Thanks to [39, Proposition H.3], the Rademacher complexities of constrained log-sum-exp quadratic functions  $x \mapsto \log u_\omega(x)$ ,  $x \mapsto \log c_\theta(x)$  and  $y \mapsto \log v_\theta(y)$  are known to be bounded by  $O(\frac{1}{\sqrt{N}})$  or  $O(\frac{1}{\sqrt{M}})$  respectively. According to the definition of Rademacher complexity, for single quadratic functions  $x \mapsto \frac{x^T x}{2}$  ( $y \mapsto \frac{y^T y}{2}$ ) it is just equal to zero. Then, using the well-known scaling and additivity properties of the Rademacher complexity [61], we get that  $x \mapsto -\varepsilon \log u_\omega(x) + \varepsilon \log c_\theta(x) - \frac{\|x\|^2}{2}$  and  $y \mapsto -\varepsilon \log v_\theta(y) - \frac{\|y\|^2}{2}$  are bounded by  $O(\frac{1}{\sqrt{N}})$  and  $O(\frac{1}{\sqrt{M}})$  respectively. The remaining step is to recall that  $\bar{f}_1(x)$  and  $\bar{f}_2(y)$  are Lipschitz. Therefore, according to Talagrand's contraction principle [47], the Rademacher complexities of  $\mathcal{F}_1$  and  $\mathcal{F}_2$  are also bounded by  $O(\frac{1}{\sqrt{N}})$  and  $O(\frac{1}{\sqrt{M}})$ , respectively.  $\square$

*Proof of Proposition 4.2.* The proof of this proposition directly follows from Propositions A.1 and A.2.  $\square$

### A.3 Proof of Theorem 4.3

To begin with, we provide a quick reminder about the Fenchel-Rockafellar theorem which is needed to derive the dual form of problem (3).

**Theorem A.3** (Fenchel-Rockafellar [56]). *Let  $(E, E')$  and  $(F, F')$  be two couples of topologically paired spaces. Let  $A : E \mapsto F$  be a continuous linear operator and  $\bar{A} : F' \mapsto E'$  be its adjoint. Let  $f$  and  $g$  be lower semicontinuous and proper convex functions defined on  $E$  and  $F$  respectively. If there exists  $x \in \text{dom} f$  s.t.  $g$  is continuous at  $Ax$ , then*

$$\sup_{x \in E} -f(-x) - g(Ax) = \min_{\bar{y} \in F'} \bar{f}(\bar{A} \bar{y}) + \bar{g}(\bar{y})$$

and the min is attained. Moreover, if there exists a maximizer  $x \in E$  then there exists  $\bar{y} \in \bar{F}$  satisfying  $Ax \in \partial \bar{g}(\bar{y})$  and  $\bar{A} \bar{y} \in \partial f(-x)$ .

We note that in the below theorem  $\mathcal{C}_2(\mathbb{R}^d)$  **does not** denote the space of twice differentiable continuous functions. The exact definition of this space and  $\mathcal{C}_{2,b}(\mathbb{R}^d)$  is given in **notations** part.

**Theorem A.4** (Dual form of problem (3)). *The primal UEOT problem (3) has the dual counterpart (4) where the potentials  $(\phi, \psi)$  belong to the space  $\mathcal{C}_{2,b}(\mathbb{R}^d) \times \mathcal{C}_{2,b}(\mathbb{R}^d)$ . The minimum of (3) is attained for a unique  $\gamma^* \in \mathcal{M}_{2,+}(\mathbb{R}^d \times \mathbb{R}^d)$ . In turn,  $\phi^*$  and  $\psi^*$  maximize (4) if and only if (5) holds true.*

*Proof.* We recall that in the primal form, the minimization is performed over functions  $\gamma$  belonging to  $\mathcal{M}_{2,+}(\mathbb{R}^d \times \mathbb{R}^d)$ . In this proof, we suppose that this space is endowed with a coarsest topology  $\sigma(\mathcal{M}_{2,+}(\mathbb{R}^d \times \mathbb{R}^d))$  which makes continuous the linear functionals  $\gamma \mapsto \int \zeta d\gamma$ ,  $\forall \zeta \in \mathcal{C}_2(\mathbb{R}^d \times \mathbb{R}^d)$ . Then the topological space  $(\mathcal{M}_{2,+}(\mathbb{R}^d \times \mathbb{R}^d), \sigma(\mathcal{M}_{2,+}(\mathbb{R}^d \times \mathbb{R}^d)))$  has a topological dual  $(\mathcal{M}_{2,+}(\mathbb{R}^d \times \mathbb{R}^d), \sigma(\mathcal{M}_{2,+}(\mathbb{R}^d \times \mathbb{R}^d)))'$  which, actually, is (linear) isomorphic to the space  $\mathcal{C}_2(\mathbb{R}^d \times \mathbb{R}^d)$ .



$\mathbb{R}^d$ ), see [26, Lemma 9.9]. This fact opens an opportunity to apply the well-celebrated Fenchel-Rockafellar theorem. For this purpose, we will consider the following spaces:  $E \stackrel{\text{def}}{=} C_2(\mathbb{R}^d) \times C_2(\mathbb{R}^d)$ ,  $F \stackrel{\text{def}}{=} C_2(\mathbb{R}^d \times \mathbb{R}^d)$  and their duals  $E' \stackrel{\text{def}}{=} \mathcal{M}_{2,+}(\mathbb{R}^d) \times \mathcal{M}_{2,+}(\mathbb{R}^d)$  and  $F' \stackrel{\text{def}}{=} \mathcal{M}_{2,+}(\mathbb{R}^d \times \mathbb{R}^d)$ .

*Step 1.* Recall that the convex conjugate of any function  $g : \mathcal{M}_{2,+}(\mathbb{R}^d \times \mathbb{R}^d) \rightarrow \mathbb{R} \cup \{+\infty\}$  is defined for each  $\zeta \in (\mathcal{M}_{2,+}(\mathbb{R}^d \times \mathbb{R}^d))' \cong C_2(\mathbb{R}^d \times \mathbb{R}^d)$  as  $\bar{g}(\zeta) = \sup_{\gamma \in \mathcal{M}_{2,+}(\mathbb{R}^d \times \mathbb{R}^d)} \{\langle \gamma, \zeta \rangle - g(\gamma)\}$ . For the convenience of further derivations, we introduce additional functionals corresponding to the summands in the primal UEOT problem (3):

$$P(\gamma) \stackrel{\text{def}}{=} \int_{\mathbb{R}^d} \int_{\mathbb{R}^d} \frac{\|x-y\|^2}{2} \gamma(x,y) dx dy - \varepsilon H(\gamma); \quad F_1(\gamma_x) \stackrel{\text{def}}{=} D_{f_1}(\gamma_x \| p); \quad F_2(\gamma_y) \stackrel{\text{def}}{=} D_{f_2}(\gamma_y \| q). \quad (24)$$

For our purposes, we need to calculate the convex conjugates of these functionals. Fortunately, convex conjugates of  $f$ -divergences  $F_1(\gamma_x)$  and  $F_2(\gamma_y)$  are well-known, see [1, Proposition 23], and equal to

$$\bar{F}_1(\phi) \stackrel{\text{def}}{=} \int_{\mathbb{R}^d} \bar{f}_1(\phi(x)) p(x) dx, \quad \bar{F}_2(\psi) \stackrel{\text{def}}{=} \int_{\mathbb{R}^d} \bar{f}_2(\psi(y)) q(y) dy.$$

To proceed, we calculate the convex conjugate of  $P(\gamma)$ :

$$\begin{aligned} \bar{P}(\zeta) &= \overline{\int_{\mathbb{R}^d} \int_{\mathbb{R}^d} \frac{\|x-y\|^2}{2} \gamma(x,y) dx dy - \varepsilon H(\gamma)} = \\ &= \sup_{\gamma \in \mathcal{M}_{2,+}(\mathbb{R}^d \times \mathbb{R}^d)} \left\{ \int_{\mathbb{R}^d} \int_{\mathbb{R}^d} \zeta(x,y) \gamma(x,y) dx dy - \left( \int_{\mathbb{R}^d} \int_{\mathbb{R}^d} \frac{\|x-y\|^2}{2} \gamma(x,y) dx dy - \varepsilon H(\gamma) \right) \right\} = \\ &= \sup_{\gamma \in \mathcal{M}_{2,+}(\mathbb{R}^d \times \mathbb{R}^d)} \left\{ \int_{\mathbb{R}^d} \int_{\mathbb{R}^d} \left( \zeta(x,y) - \frac{\|x-y\|^2}{2} \right) \gamma(x,y) dx dy + \underbrace{\varepsilon \left( \int_{\mathbb{R}^d} \int_{\mathbb{R}^d} -\gamma(x,y) \log \gamma(x,y) dx dy - 1 + \|\gamma\|_1 \right)}_{=H(\gamma)} \right\} = \\ &= \sup_{\gamma \in \mathcal{M}_{2,+}(\mathbb{R}^d \times \mathbb{R}^d)} \varepsilon \cdot \left\{ \int_{\mathbb{R}^d} \int_{\mathbb{R}^d} \gamma(x,y) \left( \frac{\zeta(x,y) - \frac{\|x-y\|^2}{2}}{\varepsilon} - \log \gamma(x,y) \right) dx dy - 1 + \int_{\mathbb{R}^d} \int_{\mathbb{R}^d} \gamma(x,y) dx dy \right\} = \\ &= \sup_{\gamma \in \mathcal{M}_{2,+}(\mathbb{R}^d \times \mathbb{R}^d)} (-\varepsilon) \cdot \left\{ \int_{\mathbb{R}^d} \int_{\mathbb{R}^d} \gamma(x,y) \left( \log \gamma(x,y) - \frac{\zeta(x,y) - \frac{\|x-y\|^2}{2}}{\varepsilon} \right) dx dy + 1 - \int_{\mathbb{R}^d} \int_{\mathbb{R}^d} \gamma(x,y) dx dy \right\} = \\ &= \sup_{\gamma \in \mathcal{M}_{2,+}(\mathbb{R}^d \times \mathbb{R}^d)} (-\varepsilon) \cdot \left\{ \int_{\mathbb{R}^d} \int_{\mathbb{R}^d} \gamma(x,y) \left( \log \gamma(x,y) - \frac{\zeta(x,y) - \frac{\|x-y\|^2}{2}}{\varepsilon} \right) dx dy + 1 - \int_{\mathbb{R}^d} \int_{\mathbb{R}^d} \gamma(x,y) dx dy + \right. \\ &\quad \left. \underbrace{\int_{\mathbb{R}^d} \int_{\mathbb{R}^d} \exp\left\{ \frac{\zeta(x,y) - \frac{\|x-y\|^2}{2}}{\varepsilon} \right\} dx dy - \int_{\mathbb{R}^d} \int_{\mathbb{R}^d} \exp\left\{ \frac{\zeta(x,y) - \frac{\|x-y\|^2}{2}}{\varepsilon} \right\} dx dy}_{=0} \right\} = \quad (25) \\ &= \sup_{\gamma \in \mathcal{M}_{2,+}(\mathbb{R}^d \times \mathbb{R}^d)} (-\varepsilon) \cdot \left\{ \mathbf{D}_{\text{KL}} \left( \gamma \parallel \exp\left\{ \frac{\zeta(x,y) - \frac{\|x-y\|^2}{2}}{\varepsilon} \right\} \right) + 1 - \int_{\mathbb{R}^d} \int_{\mathbb{R}^d} \exp\left\{ \frac{\zeta(x,y) - \frac{\|x-y\|^2}{2}}{\varepsilon} \right\} dx dy \right\}. \quad (26) \end{aligned}$$

Here in the transition from (25) to (26), we keep in mind our prior calculations of  $\mathbf{D}_{\text{KL}}$  in (20).

Recall that  $\mathbf{D}_{\text{KL}}$  is non-negative and attains zero at the unique point

$$\gamma^*(x,y) = \exp\left\{ \frac{\zeta(x,y) - \frac{\|x-y\|^2}{2}}{\varepsilon} \right\}. \quad (27)$$

Thus, we get

$$\bar{P}(\zeta) = \varepsilon \int_{\mathbb{R}^d} \int_{\mathbb{R}^d} \exp\left\{ \frac{\zeta(x,y) - \frac{\|x-y\|^2}{2}}{\varepsilon} \right\} dx dy - \varepsilon. \quad (28)$$

*Step 2.* Now we are ready to apply the Fenchel-Rockafellar theorem in our case. To begin with, we show that this theorem is applicable to problem (3), i.e., that the functions under consideration satisfy the necessary conditions. Indeed, it is known that the convex conjugate of any functional (e.g.,  $\overline{F_1}(\cdot)$ ,  $\overline{F_2}(\cdot)$ ,  $\overline{P}(\cdot)$ ) is **lower semi-continuous** and **convex**. Besides, the listed functionals are **proper convex**<sup>2</sup>. Indeed, the properness of  $\overline{F_1}(\cdot)$  and  $\overline{F_2}(\cdot)$  follows from the fact that  $f$ -divergences are known to be lower-semicontinuous and proper themselves, while properness of  $\overline{P}(\cdot)$  is evident from (26).

Now we consider the linear operator  $A : C_2(\mathbb{R}^d) \times C_2(\mathbb{R}^d) \mapsto C_2(\mathbb{R}^d \times \mathbb{R}^d)$  which is defined as  $A(\phi, \psi) : (x, y) \mapsto \phi(x) + \psi(y)$ . It is continuous, and its adjoint is defined on  $\mathcal{M}_{2,+}(\mathbb{R}^d \times \mathbb{R}^d)$  as  $\overline{A}(\gamma) = (\gamma_x, \gamma_y)$ . Indeed,  $\langle \overline{A}(\gamma), (u, v) \rangle = \langle \gamma, A(u, v) \rangle = \int_{\mathbb{R}^d} \int_{\mathbb{R}^d} \gamma(x, y)(u(x) + v(y)) dx dy = \int_{\mathbb{R}^d} \gamma_x(x)u(x) dx + \int_{\mathbb{R}^d} \gamma_y(y)v(y) dy$ .

Thus, the strong duality and the existence of minimizer for (3) follows from the Fenchel-Rockafellar theorem which states that problems

$$\sup_{(\phi, \psi) \in C_2(\mathbb{R}^d) \times C_2(\mathbb{R}^d)} \{-\overline{P}(A(\phi, \psi)) - \overline{F_1}(-\phi) - \overline{F_2}(-\psi)\} \quad (29)$$

and

$$\min_{\gamma \in \mathcal{M}_{2,+}(\mathbb{R}^d \times \mathbb{R}^d)} \{\varepsilon P(\gamma) + F_1(\gamma_x) + F_2(\gamma_y)\} \quad (30)$$

are equal. Uniqueness of the minimizer for (3) comes from the strict convexity of  $P(\cdot)$  (which holds thanks to the entropy term). Note that the conjugate of the sum of  $F_1$  and  $F_2$  is equal to the sum of their conjugates since they are defined for separate non-intersecting groups of parameters.

Next we prove that the supremum can be restricted to  $\mathcal{C}_{2,b}(\mathbb{R}^d \times \mathbb{R}^d)$ . Here we use  $\vee$  to denote the operation of taking maximum between the function  $f : \mathbb{R}^d \rightarrow \mathbb{R}$  and real value  $k$ :  $f \vee k = \{\max(f(x), k) \mid x \in \mathbb{R}^d\}$ . We observe that

$$\begin{aligned} & \sup_{(\phi, \psi) \in C_2(\mathbb{R}^2) \times C_2(\mathbb{R}^2)} \{-\varepsilon \int_{\mathbb{R}^d} \int_{\mathbb{R}^d} \exp\left\{\frac{\phi(x) + \psi(y) - \frac{\|x-y\|^2}{2}}{\varepsilon}\right\} dx dy - \overline{F_1}(-\phi) - \overline{F_2}(-\psi)\} = \\ & \lim_{k_1 \rightarrow -\infty} \lim_{k_2 \rightarrow -\infty} \sup_{(\phi, \psi) \in C_2(\mathbb{R}^2) \times C_2(\mathbb{R}^2)} \left\{-\varepsilon \int_{\mathbb{R}^d} \int_{\mathbb{R}^d} \exp\left\{\frac{\phi(x) \vee k_1 + \psi(y) \vee k_2 - \frac{\|x-y\|^2}{2}}{\varepsilon}\right\} dx dy - \right. \\ & \quad \left. \int_{\mathbb{R}^d} \overline{F_1}(\psi(x) \vee k_1) p(x) dx - \int_{\mathbb{R}^d} \overline{F_2}(\psi(x) \vee k_2) q(y) dy\right\} = \\ & \lim_{k_1 \rightarrow -\infty} \lim_{k_2 \rightarrow -\infty} \{-\overline{P}(A(\phi \vee k_1, \psi \vee k_2)) - \overline{F_1}(-\phi \vee k_1) - \overline{F_2}(-\psi \vee k_2)\}. \quad (31) \end{aligned}$$

Thus, we get

$$\begin{aligned} & \sup_{(\phi, \psi) \in C_2(\mathbb{R}^2) \times C_2(\mathbb{R}^2)} \{-\overline{P}(A(\phi, \psi)) - \overline{F_1}(-\phi) - \overline{F_2}(-\psi)\} = \\ & \sup_{(\phi, \psi) \in C_2(\mathbb{R}^2) \times C_2(\mathbb{R}^2)} \lim_{k_1 \rightarrow -\infty} \lim_{k_2 \rightarrow -\infty} \{-\overline{P}(A(\phi \vee k_1, \psi \vee k_2)) - \overline{F_1}(-\phi \vee k_1) - \overline{F_2}(-\psi \vee k_2)\} \leq \\ & \sup_{(\phi, \psi) \in \mathcal{C}_{2,b}(\mathbb{R}^2) \times \mathcal{C}_{2,b}(\mathbb{R}^2)} \{-\overline{P}(A(\phi, \psi)) - \overline{F_1}(-\phi) - \overline{F_2}(-\psi)\}. \quad (32) \end{aligned}$$

Since the other inequality is obvious, the two quantities are equal which completes the proof.  $\square$

*Proof of Theorem 4.3.* Our aim is to prove that for all  $\delta > 0$  there exist unnormalized Gaussian mixtures  $u_\omega$  and  $v_\theta$  s.t.  $\mathcal{L}(\theta, \omega) - \mathcal{L}^* < \delta\varepsilon$ . Following (18), we define

$$\mathcal{J}(\phi, \psi) \stackrel{\text{def}}{=} \varepsilon \int_{\mathbb{R}^d} \int_{\mathbb{R}^d} \exp\left\{\frac{1}{\varepsilon}(\phi(x) + \psi(y) - \frac{\|x-y\|^2}{2})\right\} dx dy + \int_{\mathbb{R}^d} \overline{F_1}(-\phi(x)) p(x) dx + \int_{\mathbb{R}^d} \overline{F_2}(-\psi(y)) q(y) dy.$$

<sup>2</sup>*Proper convex* function is a real-valued convex function which has a non-empty domain, never attains the value  $(-\infty)$  and is not identically equal to  $(+\infty)$ . This property ensures that the minimization problem for this function has non-trivial solutions.

Then from (4), it follows that  $\mathcal{L}^* = \inf_{(\phi, \psi) \in \mathcal{C}_{2,b}(\mathbb{R}^d) \times \mathcal{C}_{2,b}(\mathbb{R}^d)} \mathcal{J}(\phi, \psi)$ . Finally, using the definition of the infimum, we get that for all  $\delta' > 0$  there exist some functions  $(\widehat{\phi}, \widehat{\psi}) \in \mathcal{C}_{2,b}(\mathbb{R}^d) \times \mathcal{C}_{2,b}(\mathbb{R}^d)$  such that  $\mathcal{J}(\widehat{\phi}, \widehat{\psi}) < \mathcal{L}^* + \delta'$ . For further derivations, we set  $\delta' \stackrel{\text{def}}{=} \frac{\delta\varepsilon}{2}$  and pick the corresponding  $(\widehat{\phi}, \widehat{\psi})$ .

*Step 1.* We start with the derivation of some inequalities useful for future steps. Since  $(\widehat{\phi}, \widehat{\psi}) \in \mathcal{C}_{2,b}(\mathbb{R}^d) \times \mathcal{C}_{2,b}(\mathbb{R}^d)$ , they have upper bounds  $\widehat{a}$  and  $\widehat{b}$  such that for all  $x, y \in \mathbb{R}^d$ :  $\widehat{\phi}(x) \leq \widehat{a}$  and  $\widehat{\psi}(y) \leq \widehat{b}$  respectively. We recall that by the assumption of the theorem, measures  $p$  and  $q$  are compactly supported. Thus, there exist balls centered at  $x = 0$  and  $y = 0$  and having some radius  $R > 0$  which contain the supports of  $p$  and  $q$  respectively. Then we define

$$\begin{aligned} \widetilde{\phi}(x) &\stackrel{\text{def}}{=} \widehat{\phi}(x) - \max\{0, \max\{\|x\|^2 - R^2, \|x\|^4 - R^4\}\} \leq \widehat{\phi}(x) \leq \widehat{a}; \\ \widetilde{\psi}(y) &\stackrel{\text{def}}{=} \widehat{\psi}(y) - \max\{0, \|y\|^2 - R^2, \|y\|^4 - R^4\} \leq \widehat{\psi}(y) \leq \widehat{b}. \end{aligned}$$

We get that

$$\begin{aligned} \widetilde{\phi}(x) \leq \widehat{\phi}(x), \widetilde{\psi}(y) \leq \widehat{\psi}(y) &\implies \\ \varepsilon \int_{\mathbb{R}^d} \int_{\mathbb{R}^d} \exp\left\{\frac{1}{\varepsilon}(\widetilde{\phi}(x) + \widetilde{\psi}(y) - \frac{\|x-y\|^2}{2})\right\} dx dy &\leq \varepsilon \int_{\mathbb{R}^d} \int_{\mathbb{R}^d} \exp\left\{\frac{1}{\varepsilon}(\widehat{\phi}(x) + \widehat{\psi}(y) - \frac{\|x-y\|^2}{2})\right\} dx dy \end{aligned} \quad (33)$$

Importantly, for all  $x$  and  $y$  within the supports of  $p$  and  $q$  it holds that  $\widetilde{\phi}(x) = \widehat{\phi}(x)$  and  $\widetilde{\psi}(y) = \widehat{\psi}(y)$ , respectively. Then

$$\int_{\mathbb{R}^d} \bar{f}_1(-\widehat{\phi}(x))p(x)dx = \int_{\mathbb{R}^d} \bar{f}_1(-\widetilde{\phi}(x))p(x)dx, \quad \int_{\mathbb{R}^d} \bar{f}_2(-\widehat{\psi}(y))q(y)dy = \int_{\mathbb{R}^d} \bar{f}_2(-\widetilde{\psi}(y))q(y)dy. \quad (34)$$

Combining (33) and (34), we get that  $\mathcal{J}(\widetilde{\phi}, \widetilde{\psi}) \leq \mathcal{J}(\widehat{\phi}, \widehat{\psi}) < \mathcal{L}^* + \delta$ .

Before moving on, we note that functions  $\exp\{\widetilde{\phi}(x)/\varepsilon\}$  and  $\exp\{\widetilde{\psi}(y)/\varepsilon\}$  are continuous and non-negative. Therefore, since measures  $p$  and  $q$  are compactly supported, there exist some constants  $e_{\min}, h_{\min} > 0$  such that  $\exp\{\widetilde{\phi}(x)/\varepsilon\} > e_{\min}$  and  $\exp\{\widetilde{\psi}(y)/\varepsilon\} > h_{\min}$  for all  $x$  and  $y$  from the supports of measures  $p$  and  $q$  respectively. We keep these constants for future steps.

*Step 2.* This step of our proof is similar to [39, Theorem 3.4]. We get that

$$\begin{aligned} \exp(\widetilde{\phi}(x)/\varepsilon) &\leq \exp\left(\frac{\widehat{a} - \max\{0, \|x\|^2 - R^2\}}{\varepsilon}\right) \leq \exp\left(\frac{\widehat{a} + R^2}{\varepsilon}\right) \cdot \exp(-\|x\|^2/\varepsilon), \\ \exp(\widetilde{\psi}(y)/\varepsilon) &\leq \exp\left(\frac{\widehat{b} - \max\{0, \|y\|^2 - R^2\}}{\varepsilon}\right) \leq \exp\left(\frac{\widehat{b} + R^2}{\varepsilon}\right) \cdot \exp(-\|y\|^2/\varepsilon). \end{aligned} \quad (35)$$

From this we can deduce that  $y \mapsto \exp(\widetilde{\psi}(y)/\varepsilon)$  is a normalizable density since it is bounded by the unnormalized Gaussian density. Moreover, we see that it vanishes at the infinity. Thus, using the result [50, Theorem 5a], we get that for all  $\delta'' > 0$  there exists an unnormalized Gaussian mixture  $v_{\widetilde{\theta}} = v_{\widetilde{\theta}}(\delta'')$  such that

$$\|v_{\widetilde{\theta}} - \exp(\widetilde{\psi}/\varepsilon)\|_{\infty} = \sup_{y \in \mathbb{R}^D} |v_{\widetilde{\theta}}(y) - \exp(\widetilde{\psi}(y)/\varepsilon)| < \delta''. \quad (36)$$

Following the mentioned theorem, we can set all the covariances in  $v_{\widetilde{\theta}}$  to be scalar, i.e., define  $v_{\widetilde{\theta}}(x_1) = \sum_{k=1}^K \widetilde{\alpha}_k \mathcal{N}(x_1 | \widetilde{r}_k, \varepsilon \widetilde{\lambda}_k I)$ . for some  $K$  and  $\widetilde{\alpha}_k \in \mathbb{R}_+$ ,  $\widetilde{r}_k \in \mathbb{R}^D$ ,  $\widetilde{\lambda}_k \in \mathbb{R}_+$  ( $k \in \{1, \dots, K\}$ ). For our future needs, we set

$$\delta'' = \frac{\delta\varepsilon}{2} \cdot \left[ L_1 \cdot \frac{\varepsilon}{e_{\min}} + L_2 \cdot \frac{\varepsilon}{h_{\min}} + \varepsilon(2\pi\varepsilon)^{\frac{d}{2}} \left(1 + (\pi\varepsilon)^{\frac{d}{2}} \exp\left\{\frac{\widehat{a} + R^2}{\varepsilon}\right\}\right) \right]^{-1}.$$

For simplicity, we consider the other mixture  $v_{\theta}(y) \stackrel{\text{def}}{=} v_{\widetilde{\theta}}(y) \exp(-\frac{\|y\|^2}{2\varepsilon})$  which is again unnormalized and has scalar covariances, see the proof of [39, Theorem 3.4] for explanation. We denote the weights, means, and covariances of this mixture by  $\alpha_k \in \mathbb{R}_+$ ,  $r_k \in \mathbb{R}^D$  and  $\lambda_k \in \mathbb{R}_+$ , respectively.

We derive that

$$\begin{aligned}
& \varepsilon \int_{\mathbb{R}^d} \int_{\mathbb{R}^d} \exp\left\{\frac{1}{\varepsilon}(\tilde{\phi}(x) + \tilde{\psi}(y) - \frac{\|x-y\|^2}{2})\right\} dx dy = \varepsilon \int_{\mathbb{R}^d} \int_{\mathbb{R}^d} \exp\left\{\frac{\tilde{\phi}(x)}{\varepsilon}\right\} \exp\left\{-\frac{\|x-y\|^2}{2\varepsilon}\right\} \exp\left\{\frac{\tilde{\psi}(y)}{\varepsilon}\right\} dx dy > \\
& \varepsilon \int_{\mathbb{R}^d} \int_{\mathbb{R}^d} \exp\left\{\frac{\tilde{\phi}(x)}{\varepsilon}\right\} \exp\left\{-\frac{\|x-y\|^2}{2\varepsilon}\right\} (v_{\tilde{\theta}}(y) - \delta'') dx dy = \\
& \varepsilon \int_{\mathbb{R}^d} \int_{\mathbb{R}^d} \exp\left\{\frac{\tilde{\phi}(x)}{\varepsilon}\right\} \exp\left\{-\frac{\|x-y\|^2}{2\varepsilon}\right\} v_{\tilde{\theta}}(y) dx dy - \delta'' \varepsilon \int_{\mathbb{R}^d} \int_{\mathbb{R}^d} \exp\left\{\frac{\tilde{\phi}(x)}{\varepsilon}\right\} \exp\left\{-\frac{\|x-y\|^2}{2\varepsilon}\right\} dx dy = \\
& \varepsilon \int_{\mathbb{R}^d} \int_{\mathbb{R}^d} \exp\left\{\frac{\tilde{\phi}(x)}{\varepsilon}\right\} \exp\left\{-\frac{\|x\|^2}{2\varepsilon}\right\} \underbrace{\exp\left\{\frac{\langle x, y \rangle}{\varepsilon}\right\} \exp\left\{-\frac{\|y\|^2}{2\varepsilon}\right\} v_{\tilde{\theta}}(y)}_{=v_{\theta}(y)} dx dy - \delta'' \varepsilon \int_{\mathbb{R}^d} \int_{\mathbb{R}^d} \exp\left\{\frac{\tilde{\phi}(x)}{\varepsilon}\right\} \exp\left\{-\frac{\|x-y\|^2}{2\varepsilon}\right\} dx dy = \\
& \varepsilon \int_{\mathbb{R}^d} \exp\left\{\frac{\tilde{\phi}(x)}{\varepsilon}\right\} \exp\left\{-\frac{\|x\|^2}{2\varepsilon}\right\} \underbrace{\left(\int_{\mathbb{R}^d} \exp\left\{\frac{\langle x, y \rangle}{\varepsilon}\right\} v_{\theta}(y) dy\right)}_{=c_{\theta}(x)} dx - \delta'' \varepsilon \int_{\mathbb{R}^d} \exp\left\{\frac{\tilde{\phi}(x)}{\varepsilon}\right\} \underbrace{\left(\int_{\mathbb{R}^d} \exp\left\{-\frac{\|x-y\|^2}{2\varepsilon}\right\} dy\right)}_{=(2\pi\varepsilon)^{d/2}} dx = \\
& \varepsilon \int_{\mathbb{R}^d} \exp\left\{\frac{\tilde{\phi}(x)}{\varepsilon}\right\} \exp\left\{-\frac{\|x\|^2}{2\varepsilon}\right\} c_{\theta}(x) dx - \delta'' \varepsilon (2\pi\varepsilon)^{d/2} \int_{\mathbb{R}^d} \exp\left\{\frac{\tilde{\phi}(x)}{\varepsilon}\right\} dx > \\
& \varepsilon \int_{\mathbb{R}^d} \exp\left\{\frac{\tilde{\phi}(x)}{\varepsilon}\right\} \exp\left\{-\frac{\|x\|^2}{2\varepsilon}\right\} c_{\theta}(x) dx - \delta'' \varepsilon (2\pi\varepsilon)^{d/2} \exp\left\{\frac{\hat{a} + R^2}{\varepsilon}\right\} \int_{\mathbb{R}^d} \underbrace{\exp\left\{-\frac{\|x\|^2}{\varepsilon}\right\} dx}_{=(\pi\varepsilon)^{d/2}} = \\
& \varepsilon \int_{\mathbb{R}^d} \exp\left\{\frac{\tilde{\phi}(x)}{\varepsilon}\right\} \exp\left\{-\frac{\|x\|^2}{2\varepsilon}\right\} c_{\theta}(x) dx - \delta'' 2^{d/2} \pi^d \varepsilon^{(d+1)/2} \exp\left\{\frac{\hat{a} + R^2}{\varepsilon}\right\}. \quad (37)
\end{aligned}$$

Step 3. At this point, we will show that for every  $\delta'' > 0$ , there exists an unnormalized Gaussian mixture  $u_{\tilde{\omega}}$  which is  $\delta''$ -close to  $\exp\{\tilde{\phi}(x)/\varepsilon\}c_{\theta}(x)$ . Using the closed-form expression for  $c_{\theta}(x)$  from [39, Proposition 3.2], we get that

$$c_{\theta}(x) = \sum_{k=1}^K \alpha_k \exp\left\{-\frac{\|r_k\|^2}{2\varepsilon\lambda_k}\right\} \exp\left\{\frac{\|r_k + x\lambda_k\|^2}{2\varepsilon\lambda_k}\right\}.$$

Then

$$\begin{aligned}
\exp\left(\frac{\tilde{\phi}(x)}{\varepsilon}\right)c_{\theta}(x) & \leq \exp\left(\frac{\hat{a} - \max\{0, \|x\|^4 - R^4\}}{\varepsilon}\right)c_{\theta}(x) \leq \exp\left(\frac{\hat{a} + R^4}{\varepsilon}\right) \cdot \exp(-\|x\|^4/\varepsilon)c_{\theta}(x) = \\
& \sum_{k=1}^K \alpha_k \exp\left(\frac{\hat{a} + R^4}{\varepsilon}\right) \exp\left\{-\frac{\|r_k\|^2}{2\varepsilon\lambda_k}\right\} \cdot \exp\left(-\frac{\|x\|^4}{\varepsilon}\right) \exp\left\{\frac{\|r_k + x\lambda_k\|^2}{2\varepsilon\lambda_k}\right\} = \\
& \sum_{k=1}^K \alpha_k \exp\left(\frac{\hat{a} + R^4}{\varepsilon}\right) \exp\left\{-\frac{\|r_k\|^2}{2\varepsilon\lambda_k}\right\} \cdot \exp\left\{\frac{\|r_k + x\lambda_k\|^2 - 2\lambda_k\|x\|^4}{2\varepsilon\lambda_k}\right\}
\end{aligned}$$

From this, we see that  $\exp(\tilde{\phi}(x)/\varepsilon)c_{\theta}(x)$  tends to zero while  $x$  approaches infinity. It means that  $x \mapsto \exp(\tilde{\phi}(x)/\varepsilon)c_{\theta}(x)$  corresponds to the normalizable density. Using [50, Theorem 5a], we get that for all  $\delta'' > 0$  there exists an unnormalized Gaussian mixture  $u_{\tilde{\omega}}$  such that

$$\|u_{\tilde{\omega}} - \exp(\tilde{\phi}/\varepsilon)c_{\theta}\|_{\infty} = \sup_{x \in \mathbb{R}^D} |u_{\tilde{\omega}}(x) - \exp(\tilde{\phi}(x)/\varepsilon)c_{\theta}(x)| < \delta''. \quad (38)$$

Analogously with  $v_{\tilde{\theta}}$ , we can set all the covariances in  $u_{\tilde{\omega}}$  to be scalar, i.e., define  $u_{\tilde{\omega}} = \sum_{l=1}^L \tilde{\beta}_l \mathcal{N}(x|\tilde{\mu}_l, \varepsilon\tilde{\zeta}_l I)$  for some  $L, \tilde{\mu}_l \in \mathbb{R}^d, \tilde{\zeta}_l \in \mathbb{R}_+$  ( $l \in \{1, \dots, L\}$ ). Moreover, we consider  $u_{\omega}(x) = u_{\tilde{\omega}}(x) \exp\{-\frac{\|x\|^2}{2\varepsilon}\}$  which is again an unnormalized density with scalar covariances. We denote the weights, means, covariances of this mixture by  $\beta_l \in \mathbb{R}_+, \mu_l \in \mathbb{R}^D, \zeta_l \in \mathbb{R}_+$  respectively.

Next we recall the equation (37) and get that

$$\begin{aligned}
(37) &> \varepsilon \int_{\mathbb{R}^d} \exp\left\{-\frac{\|x\|^2}{2\varepsilon}\right\} (u_{\tilde{\omega}}(x) - \delta'') dx - \delta'' 2^{d/2} \pi^d \varepsilon^{(d+1)} \exp\left\{\frac{\hat{a} + R^2}{\varepsilon}\right\} = \\
&\varepsilon \underbrace{\int_{\mathbb{R}^d} \exp\left\{-\frac{\|x\|^2}{2\varepsilon}\right\} u_{\tilde{\omega}}(x) dx}_{=u_{\omega}(x)} - \varepsilon \delta'' \underbrace{\int_{\mathbb{R}^d} \exp\left\{-\frac{\|x\|^2}{2\varepsilon}\right\} dx}_{=(2\pi\varepsilon)^{\frac{d}{2}}} - \delta'' 2^{d/2} \pi^d \varepsilon^{(d+1)} \exp\left\{\frac{\hat{a} + R^2}{\varepsilon}\right\} = \\
&\varepsilon \|u_{\omega}\|_1 - \varepsilon \delta'' (2\pi\varepsilon)^{\frac{d}{2}} \left(1 + (\pi\varepsilon)^{\frac{d}{2}} \exp\left\{\frac{\hat{a} + R^2}{\varepsilon}\right\}\right). \quad (39)
\end{aligned}$$

*Step 4.* Now we turn to other expressions. Using the property that a function  $t \mapsto \log t$  is  $\frac{1}{t_{\min}}$ -Lipshitz on interval  $[t_{\min}, +\infty)$  we get

$$\log\left(\exp\left\{\frac{\tilde{\psi}(y)}{\varepsilon}\right\}\right) - \log\left(\exp\left\{\frac{\tilde{\psi}(y)}{\varepsilon}\right\} - \delta''\right) \leq \frac{\delta''}{h_{\min}} \implies \log\left(\exp\left\{\frac{\tilde{\psi}(y)}{\varepsilon}\right\} - \delta''\right) \geq \frac{\tilde{\psi}(y)}{\varepsilon} - \frac{\delta''}{h_{\min}}. \quad (40)$$

Similarly, we get that

$$\log\left(\exp\left\{\frac{\tilde{\phi}(y)}{\varepsilon}\right\} c_{\theta}(x) - \delta''\right) \geq \frac{\tilde{\phi}(y)}{\varepsilon} + \log c_{\theta}(x) - \frac{\delta''}{e_{\min}}. \quad (41)$$

We use this inequality, monotonicity of logarithm function, and (35), to derive

$$\begin{aligned}
v_{\tilde{\theta}}(y) &\stackrel{(35)}{>} \exp\left\{\frac{\tilde{\psi}(y)}{\varepsilon}\right\} - \delta'' \implies \log v_{\tilde{\theta}}(y) > \log\left(\exp\left\{\frac{\tilde{\psi}(y)}{\varepsilon}\right\} - \delta''\right) \stackrel{(40)}{\geq} \frac{\tilde{\psi}(y)}{\varepsilon} - \frac{\delta''}{h_{\min}} \implies \\
&-\tilde{\psi}(y) > -\varepsilon \log v_{\tilde{\theta}}(y) - \frac{\varepsilon \delta''}{h_{\min}}; \quad (42)
\end{aligned}$$

$$\begin{aligned}
u_{\tilde{\omega}}(x) &\stackrel{(38)}{>} \exp\left\{\frac{\tilde{\phi}(x)}{\varepsilon}\right\} c_{\theta}(x) - \delta'' \implies \log u_{\tilde{\omega}}(x) > \log\left(\exp\left\{\frac{\tilde{\phi}(x)}{\varepsilon}\right\} c_{\theta}(x) - \delta''\right) \stackrel{(41)}{\geq} \\
&\frac{\tilde{\phi}(x)}{\varepsilon} + \log c_{\theta}(x) - \frac{\delta''}{e_{\min}} \implies -\tilde{\phi}(x) > -\varepsilon \log \frac{u_{\tilde{\omega}}(x)}{c_{\theta}(x)} - \frac{\varepsilon \delta''}{e_{\min}}. \quad (43)
\end{aligned}$$

Recall that  $\bar{f}_1$  and  $\bar{f}_2$  are non-decreasing functions. Moreover, they are Lipshitz with the constants  $L_1, L_2$  respectively. Thus, we get

$$\begin{aligned}
\bar{f}_2(-\tilde{\psi}(y)) &> \bar{f}_2\left(-\varepsilon \log v_{\tilde{\theta}}(y) - \frac{\varepsilon \delta''}{h_{\min}}\right) = \bar{f}_2\left(-\varepsilon \log v_{\theta}(y) + \frac{\|y\|^2}{2\varepsilon} - \frac{\varepsilon \delta''}{h_{\min}}\right) = \\
&\bar{f}_2\left(-\varepsilon \log v_{\theta}(y) - \frac{\|y\|^2}{2} - \frac{\varepsilon \delta''}{h_{\min}}\right) \geq \bar{f}_2\left(-\varepsilon \log v_{\theta}(y) - \frac{\|y\|^2}{2}\right) - L_2 \cdot \frac{\varepsilon \delta''}{h_{\min}}; \quad (44) \\
\bar{f}_1(-\tilde{\phi}(y)) &> \bar{f}_1\left(-\varepsilon \log \frac{u_{\tilde{\omega}}(x)}{c_{\theta}(x)} - \frac{\varepsilon \delta''}{e_{\min}}\right) = \bar{f}_1\left(-\varepsilon \log u_{\tilde{\omega}}(x) + \varepsilon \log c_{\theta}(x) - \frac{\varepsilon \delta''}{e_{\min}}\right) = \\
\bar{f}_1\left(-\varepsilon \log u_{\omega}(x) - \frac{\|x\|^2}{2} + \varepsilon \log c_{\theta}(x) - \frac{\varepsilon \delta''}{e_{\min}}\right) &= \bar{f}_1\left(-\varepsilon \log \frac{u_{\omega}(x)}{c_{\theta}(x)} - \frac{\|x\|^2}{2} - \frac{\varepsilon \delta''}{e_{\min}}\right) \geq \\
&\bar{f}_1\left(-\varepsilon \log \frac{u_{\omega}(x)}{c_{\theta}(x)} - \frac{\|x\|^2}{2}\right) - L_1 \cdot \frac{\varepsilon \delta''}{e_{\min}}. \quad (45)
\end{aligned}$$

Integrating these inequalities over all  $x$  and  $y$  in supports of  $p$  and  $q$  respectively, we get

$$\int_{\mathbb{R}^d} \bar{f}_2(-\psi(y)) q(y) dy \geq \int_{\mathbb{R}^d} \bar{f}_2\left(-\varepsilon \log v_{\theta}(y) - \frac{\|y\|^2}{2}\right) q(y) dy - L_2 \cdot \frac{\varepsilon \delta''}{h_{\min}}; \quad (46)$$

$$\int_{\mathbb{R}^d} \bar{f}_1(-\phi(x)) p(x) dx \geq \int_{\mathbb{R}^d} \bar{f}_1\left(-\varepsilon \log \frac{u_{\omega}(x)}{c_{\theta}(x)} - \frac{\|x\|^2}{2}\right) p(x) dx - L_1 \cdot \frac{\varepsilon \delta''}{e_{\min}}. \quad (47)$$

Finally, combining (39) and (47), we get

$$\begin{aligned}
\mathcal{L}(\theta, \omega) &= \mathcal{J}(\phi_{\theta, \omega}, \psi_{\theta}) = \varepsilon \|u_{\omega}\|_1 + \overline{f_1}(-\varepsilon \log \frac{u_{\omega}(x)}{c_{\theta}(x)} - \frac{\|x\|^2}{2})p(x)dx + \overline{f_2}(-\varepsilon \log v_{\theta}(y) - \frac{\|y\|^2}{2})q(y)dy < \\
&\varepsilon \int_{\mathbb{R}^d} \int_{\mathbb{R}^d} \exp\{\frac{1}{\varepsilon}(\tilde{\phi}(x) + \tilde{\psi}(y) - \frac{\|x-y\|^2}{2})\}dxdy + \int_{\mathbb{R}^d} \overline{f_1}(-\tilde{\phi}(x))p(x)dx + \int_{\mathbb{R}^d} \overline{f_2}(-\tilde{\psi}(y))q(y)dy + \\
&L_1 \cdot \frac{\varepsilon \delta''}{e_{\min}} + L_2 \cdot \frac{\varepsilon \delta''}{h_{\min}} + \varepsilon \delta'' (2\pi\varepsilon)^{\frac{d}{2}} \left(1 + (\pi\varepsilon)^{\frac{d}{2}} \exp\left\{\frac{\hat{a} + R^2}{\varepsilon}\right\}\right) < \\
\mathcal{L}^* + \delta' + \delta'' \left[ L_1 \cdot \frac{\varepsilon}{e_{\min}} + L_2 \cdot \frac{\varepsilon}{h_{\min}} + \varepsilon (2\pi\varepsilon)^{\frac{d}{2}} \left(1 + (\pi\varepsilon)^{\frac{d}{2}} \exp\left\{\frac{\hat{a} + R^2}{\varepsilon}\right\}\right) \right] &\leq \mathcal{L}^* + \frac{\delta\varepsilon}{2} + \frac{\delta\varepsilon}{2} \implies \\
\mathbf{D}_{\text{KL}}(\gamma_{\theta, \omega} \|\gamma^*) &\leq \varepsilon^{-1}(\mathcal{L}(\theta, \omega) - \mathcal{L}^*) < \delta
\end{aligned}$$

which completes the proof.  $\square$

## B Experiments Details

### B.1 General Details

For minimization of the objective (14), we parametrize  $\alpha_k, r_k, S_k$  and  $\beta_l, \mu_l, \Sigma_l$  of  $v_{\theta}$  and  $u_{\omega}$  (11) respectively. For simplicity, we parametrize  $\alpha_k, \beta_l$  as their logarithms  $\log \alpha_k, \log \beta_l$ , variables  $r_k, \mu_l$  are parametrized directly. We consider diagonal matrices  $S_k, \Sigma_l$  and parametrize them via the values  $\log(S_k)_{i,i}, \log(\Sigma_l)_{i,i}$  respectively. We initialize the parameters following the scheme in [39]. In all experiments, we use Adam optimizer and set  $K = L$ .

### B.2 Details on Experiment with Gaussian Mixtures

For our solver we use  $K = L = 5, \varepsilon = 0.05, lr = 3e - 4$  and batchsize 128. We do  $2 \cdot 10^4$  gradient steps.

**Baselines.** For the OT-FM and UOT-FM methods, we parameterize the vector field  $(v_{t, \theta})_{t \in [0,1]}$  for mass transport using a 1-layer feed-forward network with 64 neurons and ReLU activation. These methods are built on the solutions (plans  $\pi^*(x, y)$ ) of discrete OT problems, to obtain them we use the POT [21] package. Especially for the UOT-FM, we use the `ot.unbalanced.sinkhorn` with the regularization equal to 0.05. We set the number of training and inference time steps equal to 100. For the LightSB algorithm, we use the parameters presented by the authors in the official repository.

### B.3 Details on Image Translation Experiment

We use the code and decoder model from

<https://github.com/podgorskiy/ALAE>

We download the data and neural network extracted attributes for the FFHQ dataset from

<https://github.com/ngushchin/LightSB/>

In the *Adult* class we include the images with the attribute  $Age \geq 44$ ; in the *Young* class - with the  $Age \in [16, 44]$ . We excluded the images with faces of children to increase the accuracy of classification per *gender* attribute. For the experiments with our solver, we use weighted  $\mathbf{D}_{\text{KL}}$  divergence with  $\tau = 100$  and set  $K = L = 50, \varepsilon = 0.1, lr = 1$ , and batch size 128. We do  $5 \cdot 10^3$  gradient steps.

**Classifier.** We trained an MLP classifier to distinguish images of the classes (*Adult, Young, Woman, Man*) to measure the accuracy of keeping the class of the input images by different solvers.

**Baselines.** For the OT-FM and UOT-FM methods, we parameterize the vector field  $(v_{t, \theta})_{t \in [0,1]}$  for mass transport using a 2-layer feed-forward network with 512 hidden neurons and ReLU activation. An additional sinusoidal embedding[63] was applied for the parameter  $t$ . Other parameters were set similarly to the *Gaussian Mixture* experiment. While both UOT-SB and UOT-GAN methods were not previously applied to the FFHQ dataset, we set up a grid search for the parameters and followed

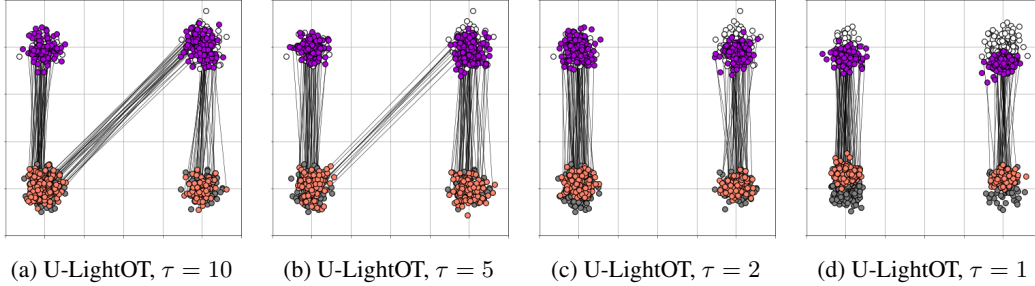


Figure 3: Conditional plans  $\gamma_{\theta,\omega}(y|x)$  learned by our solver with scaled  $D_{\chi^2}$  divergences in *Gaussians Mixture* experiment ( $\tau \in [1, 2, 5, 10]$ ).

the instructions provided by the authors for parameter settings. For UOT-SB and UOT-GAN, we used a 3-layer neural network with 512 hidden neurons, and ReLU activation was used for the generator networks and the potential and discriminator, respectively. A learning rate of  $1 \times 10^{-5}$  with the Adam optimizer was used to train the networks in UOT-SB, and a learning rate equal to  $1 \times 10^{-4}$  was used for UOT-GAN. The methods were trained for 10k iterations with a batch size equal to 128, and the best results achieved during the evaluation steps were reported. Divergence used for UOT-SB is KL. All other parameters were set to the default values provided by the authors for CIFAR-10 generation tasks.

### C Ablation Studies

**Details about  $f$ -divergences between positive measures.** In the classic form,  $f$ -divergences are defined as measures of dissimilarity between two *probability* measures. This definition should be revised when dealing with measures of arbitrary masses. Below we show that if the function  $f$  is convex, non-negative, and attains zero uniquely at point  $\{1\}$  then  $D_f(\mu_1||\mu_2)$  is a valid measure of dissimilarity between two positive measures.

Let  $\mu_1, \mu_2 \in \mathcal{M}_{2,+}(\mathbb{R}^{d'})$  be two positive measures. The  $f$ -divergence  $D_f(\mu_1||\mu_2) \geq 0$  which is obvious from the non-negativity of  $f$ . From the definition of  $D_f(\mu_1||\mu_2)$  and the fact that function  $f$  attains zero uniquely at a point  $\{1\}$ , we obtain that  $D_f(\mu_1||\mu_2) = 0$  if and only if  $\mu_1 = \mu_2$ . Then from the definition of  $D_f(\mu_1||\mu_2)$ , its non-negativity and properties of function  $f$  (it attains zero uniquely at a point  $\{1\}$ ) we get that  $D_f(\mu_1||\mu_2) = 0$  if and only if  $\mu_1 = \mu_2$ . It completes the proof.

We assessed the performance of our solver with scaled  $D_{KL}$  divergences in the main text, see §5.1, §5.2. For completeness, below we evaluate our solver with  $D_{\chi^2}$  divergence in *Gaussian Mixture* experiment. We use the same experimental setup as in §5.1. Interestingly, the solver’s results differ from those which we obtain for  $D_{KL}$  divergence. For  $D_{\chi^2}$  divergence, supports of learned plans’ marginals constitute only parts of source and target measures’ supports when  $\tau = 1$ . The issue disappears with a slight increase of  $\tau$ , i.e., for  $\tau = 2$ . At the same time, a further increase of  $\tau$  is useless, since the learned plans fail to deal with class imbalance issue. Thus, parameter  $\tau$  should be adjusted heuristically. In the case of  $D_{KL}$  divergence, supports coincide for all  $\tau$ , see Fig. 1. This motivates us to use  $D_{KL}$  divergences in our main experiments.

*Remark 1.* By definition, convex conjugates of  $D_{KL}$  and  $D_{\chi^2}$  divergences are proper, non-negative and non-decreasing. These properties are used in some of our theoretical results.

*Remark 2.* For scaled divergences  $\tau D_f$  the convex conjugates of generator functions  $\tau \cdot f$  equal to  $\tau \cdot \overline{f}(\frac{t}{\tau})$  (it is a well-known property of  $f$ -divergences). Notably, in the case of scaled  $D_{\chi^2}$  divergence, the changes are more tricky, i.e.,  $\tau \cdot \overline{f_{\chi^2}}(t) = \mathbb{I}_{t < -2\tau} \cdot (-\tau) + \mathbb{I}_{t \geq -2\tau} \cdot (0.25t^2 + t)$ .

**Parameters  $\tau, \varepsilon$ .** The effect of entropy regularization parameter  $\varepsilon$  is well studied, see, e.g., [28, 39]. Namely, increasing the parameter  $\varepsilon$  stimulates the conditional distributions  $\gamma_{\theta}(y|x)$  to become more dispersed. Still, below we provide an additional quantitative analysis of its influence on the learned translation. An ablation study on unbalancedness parameter  $\tau$  in *Gaussian Mixture* experiment is conducted in §5.1 and above in this section. However, one may naturally wonder *how this parameter will influence the performance of our solver in image translation experiments?* To address this question, we learn the translations *Young*  $\rightarrow$  *Adult*, *Man*  $\rightarrow$  *Woman* on FFHQ dataset varying the

parameters  $\tau$ ,  $\varepsilon$ , see §5.2 for the experimental setup details. We test our solver with scaled  $D_{\text{KL}}$  divergence training it for 3K iterations. Other hyperparameters are in Appendix B. In Tables 4, 6, we report the accuracy of keeping the attributes of the source images (e.g., gender in *Young*→*Adult* translation). In Tables 5, 7, we report FD metrics which is defined as *Frechet distance* between means and covariances of the learned and the target measures.

$\varepsilon \backslash \tau$	10	20	50	$10^2$	$10^3$	$10^6$
0.01	96.44 ± 0.08	96.09 ± 0.07	93.83 ± 0.12	90.30 ± 0.95	81.98 ± 0.20	80.05 ± 0.8
0.1	94.90 ± 0.34	94.23 ± 0.03	91.85 ± 0.47	88.77 ± 0.57	80.85 ± 0.77	77.80 ± 0.28
0.5	89.15 ± 0.52	87.42 ± 0.40	84.39 ± 0.91	80.32 ± 0.40	71.77 ± 0.68	71.21 ± 0.57
1.0	–	81.20 ± 0.44	77.92 ± 0.45	75.09 ± 0.21	67.08 ± 0.64	66.12 ± 0.42

Table 4: Test accuracy ( $\uparrow$ ) of keeping the class in *Young* → *Adult* translation.

$\varepsilon \backslash \tau$	10	20	50	$10^2$	$10^3$	$10^6$
0.01	35.58 ± 0.61	28.48 ± 1.20	19.33 ± 3.09	15.12 ± 1.92	12.31 ± 1.01	10.95 ± 0.03
0.1	46.90 ± 0.94	40.76 ± 1.68	45.75 ± 18.63	28.01 ± 0.77	27.96 ± 3.75	27.68 ± 1.35
0.5	114.93 ± 1.27	105.48 ± 0.66	99.00 ± 5.39	92.65 ± 0.79	89.71 ± 1.35	89.28 ± 0.53
1.0	–	168.18 ± 3.75	150.95 ± 0.55	143.08 ± 0.69	136.61 ± 0.97	137.26 ± 2.18

Table 5: Test FD ( $\downarrow$ ) of generated latent codes in *Young* → *Adult* translation.

$\varepsilon \backslash \tau$	10	20	50	$10^2$	$5 \cdot 10^2$	$10^3$	$10^6$
0.01	96.33 ± 0.35	96.08 ± 0.11	93.28 ± 0.65	89.36 ± 0.54	83.85 ± 0.84	81.57 ± 1.36	79.87 ± 0.21
0.1	94.79 ± 0.13	93.88 ± 0.47	91.60 ± 0.25	88.59 ± 0.40	81.14 ± 1.56	78.70 ± 0.84	78.92 ± 1.20
0.5	88.75 ± 0.72	88.11 ± 0.14	86.03 ± 0.72	81.34 ± 0.74	75.09 ± 1.02	73.71 ± 1.16	71.53 ± 0.58
1.0	–	81.28 ± 1.02	78.72 ± 0.89	75.15 ± 1.26	70.99 ± 0.68	68.26 ± 1.75	66.95 ± 1.26

Table 6: Test accuracy ( $\uparrow$ ) of keeping the class in *Man* → *Woman* translation.

$\varepsilon \backslash \tau$	10	20	50	$10^2$	$5 \cdot 10^2$	$10^3$	$10^6$
0.01	79.86 ± 6.94	68.80 ± 3.17	62.00 ± 12.65	69.13 ± 21.26	40.30 ± 7.22	38.20 ± 3.63	32.47 ± 0.62
0.1	89.42 ± 0.10	91.44 ± 14.59	67.07 ± 2.53	89.87 ± 39.27	50.36 ± 0.89	67.79 ± 13.59	48.46 ± 0.25
0.5	161.30 ± 2.23	148.66 ± 1.45	137.93 ± 5.64	125.50 ± 0.38	117.95 ± 0.09	117.25 ± 0.80	130.64 ± 21.15
1.0	–	212.39 ± 3.33	198.20 ± 9.68	187.03 ± 12.06	186.33 ± 15.09	174.32 ± 13.00	163.90 ± 0.28

Table 7: Test FD ( $\downarrow$ ) of generated latent codes in *Man* → *Woman* translation.

*Results* show that increase of  $\varepsilon$  negatively influences both accuracy and FD of generated latent codes which is caused by an increased dispersity of  $\gamma_{\theta}(y|x)$ . At the same time, when  $\tau$  increases, the learned plans provide *worse accuracy* for keeping the input latents’ class but *better FD* of generated latent codes. It is an expected behavior since for bigger  $\tau$ , the constraints on the marginals of the learned plans become more strict. That is, we enforce the marginals of the learned plans to be closer to source and target measures which allows learning more accurate mappings to target measure but does not allow keeping the source classes in the case of imbalance issues. Interestingly, in *Young*→*Adult* translation, FD of learned latents do not change much for  $\tau \geq 10^2$  while accuracy exhibits a significant drop between  $\tau = 10^2$  and  $\tau = 10^3$ . Thus, we can treat  $\tau = 10^2$  as optimal since it provides the best tradeoff between the quality of learned translations and their ability to keep the features of input latents. In the case of *Man*→*Woman* translation, the values of accuracy and FD exhibit significant differences for considered  $\tau$ . It shows the necessity to consider a more detailed scale where we can choose  $\tau = 5 \cdot 10^2$  as the optimal one.

*Remark.* FD should be treated as a *relative* measure of similarity between learned and target measures. The results obtained by balanced solver [39, LightSB] (equivalent to ours for big  $\tau$ ) are considered as a gold standard.

## D Limitations and Broader Impact

**Limitations.** One limitation of our solver is the usage of the Gaussian Mixture parametrization which might restrict the scalability of our solver. This points to the necessity for developing ways to optimize objective (4) with more general parametrization, e.g., neural networks. This is a promising avenue for future work.

**Broader impact.** Our work aims to advance the field of Machine Learning. There are many potential societal consequences of our work, none of which we feel must be specifically highlighted here.



## E Additional Experimental Results

We give additional illustrations for our U-LightOT solver and its alternatives applied in the latent space of ALAE autoencoder in Figures 5,4, 6, 7.



Figure 4: Comparison of solvers, *Young*  $\rightarrow$  *Adult* translation.



Figure 5: Comparison of solvers, *Adult*→*Young* translation.

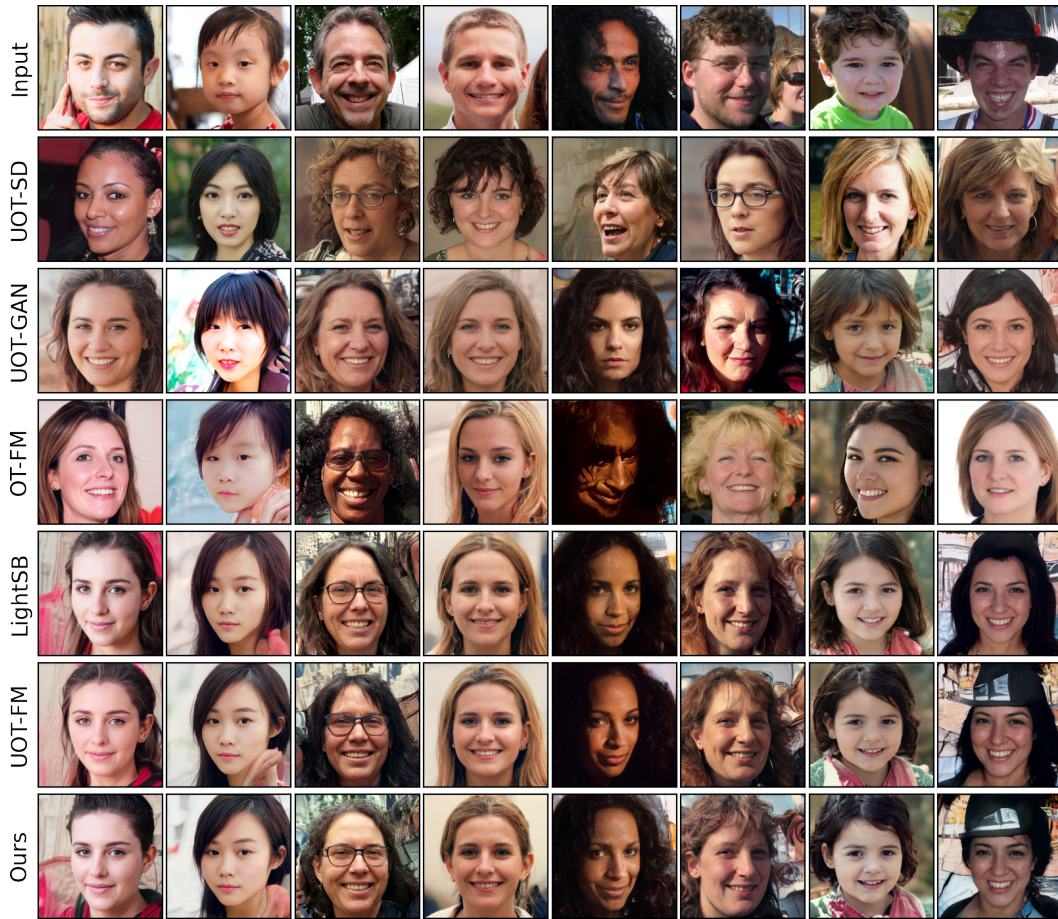


Figure 6: Comparison of solvers, *Man*→*Woman* translation.

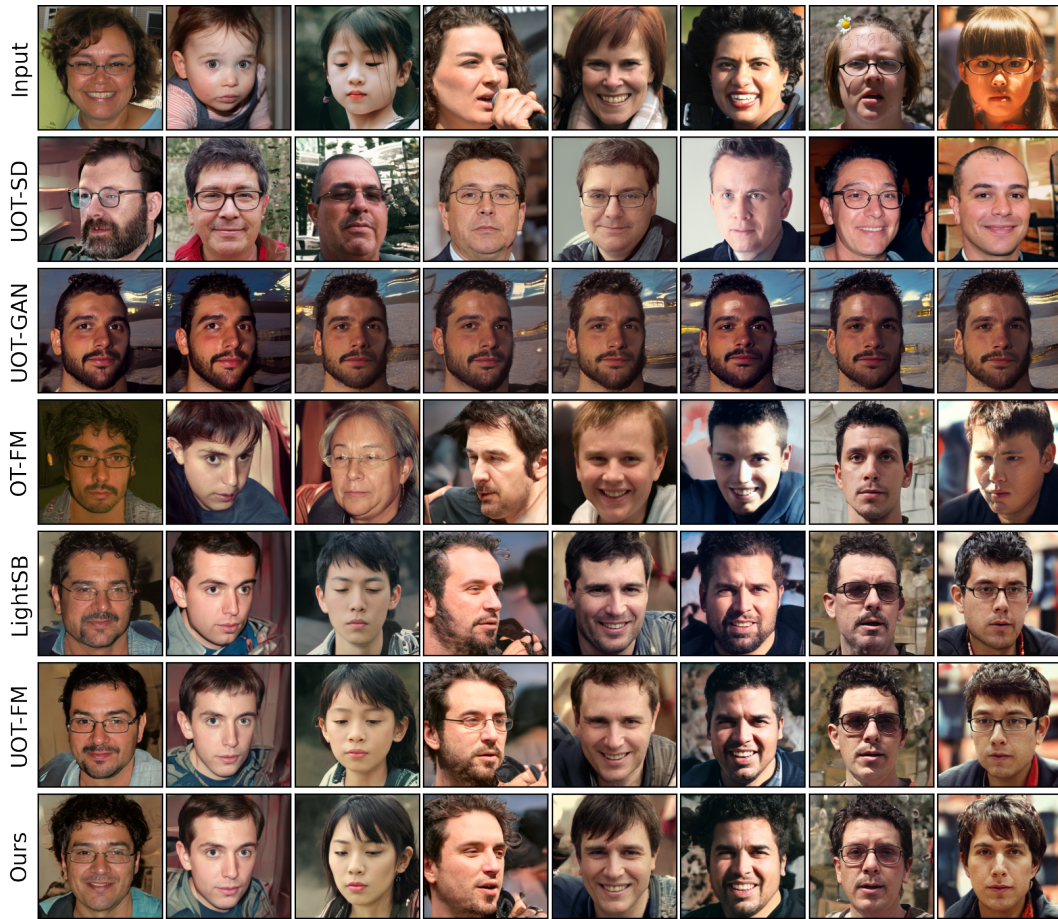


Figure 7: Comparison of solvers, *Woman*→*Man* translation.